Superconductor
Science and
Technology

PAPER • **OPEN ACCESS**

Analytical and numerical computation of AC loss in multifilament MgB_2 wires under arbitrarily time-varying transverse magnetic field

To cite this article: Calvin C T Chow *et al* 2025 *Supercond. Sci. Technol.* **38** 075005

OPEN ACCESS
IOP Publishing
Superconductor Science and Technology
Supercond. Sci. Technol. **38** (2025) 075005 (20pp)
https://doi.org/10.1088/1361-6668/add8c4

Analytical and numerical computation of AC loss in multifilament MgB_2 wires under arbitrarily time-varying transverse magnetic field

Calvin C T Chow[1,2], **Mark D Ainslie**[3] and **K T Chau**[1,*]

[1] Research Centre for Electric Vehicles and Department of Electrical and Electronic Engineering, The Hong Kong Polytechnic University, Hung Hom, Kowloon, Hong Kong Special Administrative Region of China, People's Republic of China
[2] Previously at Department of Electrical and Electronic Engineering, The University of Hong Kong, Pokfulam, Hong Kong Special Administrative Region of China, People's Republic of China
[3] Department of Engineering, Faculty of Natural, Mathematical and Engineering Sciences, King's College London, WC2R 2LS London, United Kingdom

E-mail: k.t.chau@polyu.edu.hk

Received 23 December 2024, revised 25 March 2025
Accepted for publication 7 May 2025
Published 24 June 2025

Abstract

Multifilament MgB_2 wires can be used in electrical machines, in which the wires experience a time-varying transverse external magnetic field that is rotating (thus consists of two orthogonal components). Analytical formulae are available in the literature to calculate the instantaneous coupling loss, eddy current loss and hysteresis loss of a multifilament superconducting wire under the action of a time-varying external magnetic field in one direction. This paper extends those formulae to the situation when the wire is subject to a time-varying external magnetic field in two orthogonal directions transverse to the wire's longitudinal axis, by deriving from first principles the instantaneous loss formulae. The coupling loss in the filament-matrix zone is derived using the anisotropic continuum model, which treats the filament-matrix zone as a continuum with anisotropic resistivity, and this removes the need to model filaments individually. The loss formulae derived are verified by numerical simulations done in the finite-element software COMSOL Multiphysics using an external magnetic field that is realistic in an electrical machine environment. Reasonable agreement can be seen between analytical and numerical calculations. In the numerical calculations, the anisotropic continuum model is implemented in 2D and 3D in COMSOL via the *H*-formulation, with almost identical results, but the 2D simulations are significantly faster than the 3D simulations.

Keywords: MgB_2, ac loss, magnetisation loss, anisotropic continuum model

* Author to whom any correspondence should be addressed.

1. Introduction

Multifilament superconducting wires have a variety of applications. In particular, MgB_2 wires can be used in the armature of superconducting machines [1, 2], because MgB_2 wires can be wound more easily than flat wires like high-temperature superconducting coated conductors, and the multifilament structure with twisting of the filaments can help reduce ac loss. Superconducting machines have high power densities, which make them attractive for use on electric aircraft or wind turbine generators [3, 4]. When superconductors are placed under a time-varying magnetic field or transport ac current, they dissipate losses collectively known as ac loss. In machines and in many other applications, it is important to estimate the ac loss in order to calculate cooling requirements and efficiency. This article focuses on the magnetisation loss of a multifilament wire, i.e. losses in the wire caused by a time-varying external magnetic field, which is likely to be the dominant form of loss [5]. In particular, it focuses on the case when the external magnetic field has two orthogonal directions, both transverse to the wire's longitudinal axis. This is experienced, for example, in a machine when the armature superconductors experience a rotating magnetic field, which changes in direction and magnitude, and may contain harmonics, and the direction has two orthogonal components. Expressions for instantaneous power dissipation are derived, and these can be integrated over time to find the energy loss over one cycle of field variation. Appendix A comments on the prevalent approach for calculating the total loss as the sum of magnetisation loss (loss due to magnetic field in the absence of transport ac current) and transport ac loss (loss due to transport ac current in the absence of magnetic field).

A multifilament wire typically consists of filaments (with a sheath) embedded in a normally conducting metal matrix, which in turn is enclosed by a normally conducting metal outer sheath. Modelling such a composite material is difficult due to the many fine filaments present (approximately 10–25 μm for MgB_2 filaments reported in [6] and 3 μm for NbTi and Nb_3Sn filaments [7]), often twisted. Magnetisation loss in a multifilament wire can be classified into different components related to this particular wire architecture: hysteresis loss in superconducting filaments, coupling loss due to current paths that include both superconducting filaments and normal matrix, and eddy current loss in the outer sheath. Some wires may also have magnetic materials (e.g. nickel and monel) and thus a ferromagnetic hysteresis loss contribution to the total loss, but due to the complexity of how magnetic materials affect the current distribution, we only consider wires without magnetic materials in this paper.

To model coupling loss in the filament-matrix zone, the anisotropic continuum model has been proposed in the literature, which removes the need to model filaments individually. Carr [8, chapter 9.2] derived an expression for the coupling loss due to an external magnetic field when the magnetic field is in one direction. This paper derives from first principles, similar to that in [8, chapter 9.2], the expression for the coupling loss when the field is in two directions.

To model the eddy current loss in the outer sheath, Turck [9] derived an expression for the eddy current loss due to an external magnetic field when the magnetic field is in one direction. This paper derives from first principles, similar to that in [9], the expression for eddy current loss when the field is in two directions.

The hysteresis loss of superconducting filaments in a multifilament wire can be calculated from the expression for a superconducting cylinder in isolation under the same magnetic field multiplied by the fill factor [8, p.127]. Thus, this paper derives an expression for the hysteresis loss of a circular superconducting wire under an external magnetic field in two directions. Our derivation is based on the one given in [8, chapter 7.3] for a field in one direction. However, the resulting expression is more complex than that for a field in one direction given in [8, chapter 7.3] and cannot be obtained by any obvious substitution of the $|\dot{B}_a|$ term in the expression for loss due to the field in one direction. Instead, derivation from first principles, like [8, chapter 7], is needed as provided in this paper.

To verify the derived formulae, numerical simulations are carried out using two models built in the finite-element software COMSOL Multiphysics. (1) In one model, we simulate the filament-matrix zone and the outer sheath, and apply the anisotropic continuum model to the filament-matrix zone. This model is used to verify the analytical coupling loss and eddy current loss expressions derived in this paper. Zhao *et al* [10] implemented the anisotropic continuum model in 3D via the H-formulation in COMSOL, but we find that the anisotropic continuum model can actually be implemented numerically in 2D as there is no z dependence. Klimenko *et al* [11] also developed a computer program to calculate electrodynamics of multifilament conductors based on a 2D anisotropic continuum model. (2) In another COMSOL model, only a superconducting wire in air is simulated (via the quasi critical state model (QCSM)), and this is used to verify the hysteresis loss formula derived (using the critical state model) in this paper.

There have also been other numerical methods proposed in the literature to model multifilament superconductor wires. The 3D geometry due to twisted filaments makes simulations quite complicated and time-consuming. Escamez *et al* [12] modelled in 3D 36 filaments using several software packages. Arsenault *et al* [13] used the H-ϕ formulation to model twisted filaments in 3D in COMSOL. Qiao *et al* [5] used the H-formulation to model MgB_2 wires with 2 and 54 twisted filaments in COMSOL in 3D and systematically investigated the effect of factors such as twist pitch and matrix resistivity on the magnetisation loss of the wire. Kameni *et al* [14] used the Frenet frame to transform 3D twisted filaments into straight filaments in 3D space to calculate magnetisation loss. Lyly *et al* [15] used a homogenised technique to model filament bundles in a NbTi wire, where the resistivity in the homogenised bundle area was a weighted sum (weighted by the volume of materials) of the resistivities of the superconducting filaments and the metal matrix. The authors in [15] assumed the filaments were untwisted and so 2D models were used and there was good agreement (difference 1%–28%) between the

homogenised model and the model in which individual filaments were modelled. Dular *et al* [16] modelled individual filaments in a matrix in the helicoidal coordinate system, which reduced the geometry from 3D to 2D. The approach was valid for 'helicoidally symmetric boundary conditions (e.g. an axial external magnetic field, with or without transport current)', and for such conditions, the hysteresis loss in the superconductor (with non-linear power-law resistivity) and coupling loss in the matrix could be modelled in one model. In the case of a transverse magnetic field, the boundary condition was no longer helicoidally symmetric, and valid results were only available for linear materials. Thus, the filaments' resistivity was set to a very low value compared to matrix's resistivity, and the resulting model could model the coupling loss in the matrix, but not the hysteresis loss in the filaments.

Regarding analytical modelling of ac loss in multifilament wires under a transverse field in two directions, Balachandran *et al* [17, 18] provided expressions for instantaneous hysteresis loss, coupling loss and eddy current loss by adapting formulae in the literature. Numerical simulations assuming isotropic resistivities in the matrix and sheath were carried out [17], and experimental results were provided for validation [18]. This paper derives loss formulae from first principles and arrives at loss expressions that are different. We use the anisotropic continuum model for coupling loss and calculate eddy current loss in the sheath considering the effect of the filament-matrix zone.

In summary, this paper contributes in the following ways. For an external magnetic field in two orthogonal directions transverse to the wire axis, this paper

- derives expressions for instantaneous coupling loss and eddy current loss of an MgB_2 multifilament wire assuming the anisotropic continuum model in the filament-matrix zone, and provides COMSOL simulations to verify the formulae (the COMSOL simulations also use the anisotropic continuum model for the filament-matrix zone);
- compares 3D and 2D implementations of the anisotropic continuum model via the H-formulation in COMSOL for simulating MgB_2 multifilament wire, to verify that a 2D model can be used instead of 3D;
- derives an expression for instantaneous hysteresis loss of an MgB_2 filament in air in isolation based on the critical state model, and verify the formula by COMSOL simulation based on the QCSM.

The rest of the paper is organised as follows. Section 2 derives expressions for the coupling loss of the filament-matrix zone, eddy current loss in the outer metal sheath, and hysteresis loss of a circular superconducting wire under an external magnetic field in two directions. Section 3 details the numerical COMSOL models used in this paper to verify the analytical formulae. Section 4 compares the analytical calculations with numerical calculations. Section 5 provides discussions and we conclude in section 6.

2. Analytical modelling

Consider a multifilament MgB_2 wire with a cross-section in the x–y plane and the conductor's length along in the $\hat{\mathbf{z}}$ direction, as shown in figure 1. The wire consists of (1) MgB_2 filaments in a normal-metal matrix, forming a filament-matrix zone, which is of radius R_f; and (2) a normal-metal sheath with inner radius R_f and outer radius R_0. The twist pitch of the filaments is L. Appendix B describes some features of practical MgB_2 wires and their relations to the models used in this paper.

Suppose the wire is subject to a time-varying magnetic field $\mathbf{B_a} = \mu_0\mathbf{H_a} = \mu_0(H_{a,x}(t)\hat{\mathbf{x}} + H_{a,y}(t)\hat{\mathbf{y}}) = B_{a,x}(t)\hat{\mathbf{x}} + B_{a,y}(t)\hat{\mathbf{y}}$ with two orthogonal components whilst carrying no transport current. There are three loss components: the hysteresis loss in superconducting filaments, the coupling loss due to coupling current that flows in the matrix and through the superconducting filaments, and eddy current loss in the normal metal sheath.

2.1. Coupling loss

2.1.1. Anisotropic continuum model. The anisotropic continuum model is used in this section 2.1 to model the filament-matrix zone. The theory of the model from [8, chapter 8] is reproduced as follows.

First, the three orthogonal axes in a new coordinate system (helical coordinate system) for the continuum are defined as follows and illustrated in figure 2. The continuum has helical symmetry due to the twisted filaments. A small displacement along a filament is described in cylindrical coordinates (r, θ, z) by

$$\begin{aligned}\mathrm{d}\mathbf{s} &= \mathrm{d}z\,\hat{\mathbf{a}}_\mathbf{z} + r\,\mathrm{d}\theta\,\hat{\mathbf{a}}_\theta \\ &= \mathrm{d}z\left(\hat{\mathbf{a}}_\mathbf{z} + r\frac{\mathrm{d}\theta}{\mathrm{d}z}\hat{\mathbf{a}}_\theta\right) \\ &= \mathrm{d}z\left(\hat{\mathbf{a}}_\mathbf{z} + r\frac{2\pi}{L}\hat{\mathbf{a}}_\theta\right).\end{aligned} \tag{1}$$

Define a unit vector along the filament axis,

$$\hat{\mathbf{a}}_\parallel := \frac{\mathrm{d}\mathbf{s}}{\mathrm{d}s} = \frac{\hat{\mathbf{a}}_\mathbf{z} + \frac{2\pi r}{L}\hat{\mathbf{a}}_\theta}{\sqrt{1 + \left(\frac{2\pi r}{L}\right)^2}}. \tag{2}$$

Since the first orthogonal vector does not have a component in $\hat{\mathbf{a}}_r$, the second orthogonal unit vector is

$$\hat{\mathbf{a}}_2 = \hat{\mathbf{a}}_r. \tag{3}$$

Finally, the third orthogonal vector is

$$\hat{\mathbf{a}}_3 = \hat{\mathbf{a}}_\parallel \times \hat{\mathbf{a}}_2 = \frac{\hat{\mathbf{a}}_\theta - \frac{2\pi r}{L}\hat{\mathbf{a}}_\mathbf{z}}{\sqrt{1 + \left(\frac{2\pi r}{L}\right)^2}}. \tag{4}$$

We treat the filament-matrix zone as a material with relative permeability $\mu_r = 1$ when calculating eddy current loss [8, p.126]. The properties in the $\hat{\mathbf{a}}_2$ and $\hat{\mathbf{a}}_3$ directions are

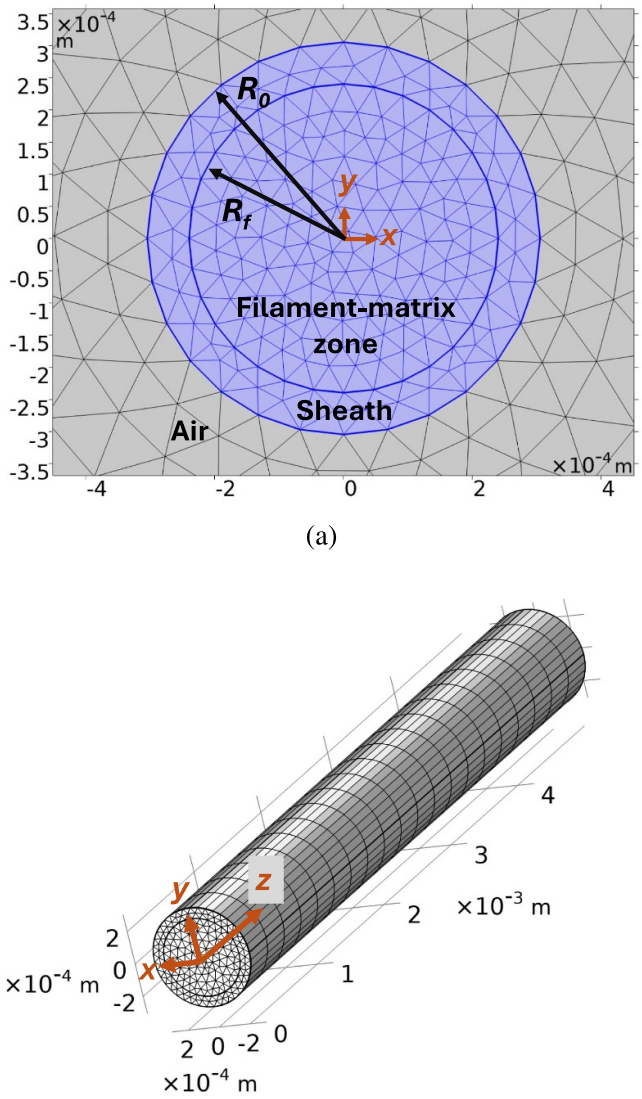

Figure 1. (a) 2D model of the multifilament wire simulated in COMSOL; the air region is the grey area surrounding the wire, which consists of the filament-matrix zone and the outer sheath. (b) 3D model simulated in COMSOL, but the air region is not shown.

assumed to be the same for simplicity [8, p.114]. Let $\rho_\perp$ be the transverse resistivity, which is the resistivity in the direction transverse to the filament axis. In the filament-matrix zone, [8, p.115]

$$\mathbf{E}_\perp = \rho_\perp \mathbf{J}_\perp, \tag{5}$$

where $\mathbf{E}_\perp$ and $\mathbf{J}_\perp$ are sum of the electric field and current density components, respectively, in the directions $\hat{\mathbf{a}}_2$ and $\hat{\mathbf{a}}_3$ transverse to the filament axis.

2.1.2. Coupling loss due to an external field with two orthogonal directions. To calculate the coupling loss in the matrix, we adapt the method in [8, chapter 9.2], which calculates

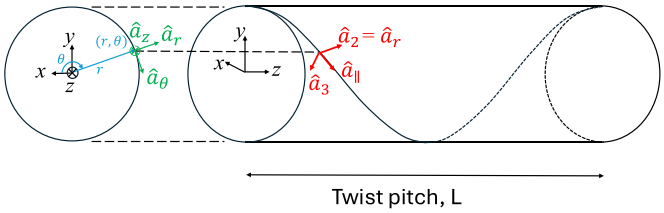

Figure 2. Illustration of a twisted filament and the coordinate system used for anisotropic continuum model (which is shown in red). The cylindrical coordinate system is shown in green. The Cartesian coordinate system is shown in black. Adapted with permission from [8], which is © [2001] Taylor & Francis Group.

the magnetisation loss of an infinitely long, twisted (twist pitch L), circular multifilament conductor with a filament-matrix zone of radius R_f subject to an external magnetic field that is: transverse to the wire; in one direction; and changes slowly enough such that it is not shielded but fully penetrates the conductor, thus $\dot{\mathbf{B}} = \mu_0 \dot{\mathbf{H}}_a$ in the continuum. Note that shielding does not occur at zero frequency due to resistance along the $\hat{\mathbf{z}}$ direction but can occur at a high frequency when the induced current cannot relax [8, p. 126]. The frequency at which the induced current cannot relax is [8, pp. 132–133]

$$f_1 = \frac{4\pi\rho_\perp}{\mu_0 L^2}, \tag{6}$$

which is approximately 20 kHz using the wire parameters in table 2, and this is well above the frequencies in a typical machine. Whilst no sheath is considered in [8, chapter 9.2], here we also assume that the current induced in the sheath still does not shield the filament-matrix zone. A relative permeability $\mu_r = 1$ is also assumed, which is valid for fine filaments or a small fill factor λ [8, p.126]. Here, we extend the approach to the case when the external field is in two directions.

From Faraday's Law $\nabla \times \mathbf{E} = -\dot{\mathbf{B}}$, in the continuum,

$$\nabla \times \mathbf{E} = -\mu_0 \dot{\mathbf{H}}_\mathbf{a} \tag{7}$$

$$\mathbf{E} = \begin{bmatrix} E_x \\ E_y \\ E_z \end{bmatrix} = \begin{bmatrix} c_x(x) \\ c_y(y) \\ -\mu_0 \dot{H}_{a,x} y + \mu_0 \dot{H}_{a,y} x + c_z(z) \end{bmatrix}, \tag{8}$$

where $c_x(x), c_y(y)$ and $c_z(z)$ are functions in x, y and z, respectively.

The expressions $c_x(x), c_y(y)$ and $c_z(z)$ can be determined by forcing $\mathbf{E} \cdot \hat{\mathbf{a}}_\parallel = 0$ ($\mathbf{E}_\parallel$ neglected for calculating the coupling loss for unsaturated transport current in a filament [8, p.115]), as follows.

Substituting $\hat{\mathbf{a}}_\theta = \frac{-y\hat{\mathbf{x}}+x\hat{\mathbf{y}}}{\sqrt{x^2+y^2}} = \frac{-y\hat{\mathbf{x}}+x\hat{\mathbf{y}}}{r}$ into (2), $\hat{\mathbf{a}}_\parallel$ can be expressed in Cartesian coordinates as

$$\hat{\mathbf{a}}_\parallel = \frac{1}{\sqrt{1+\left(\frac{2\pi r}{L}\right)^2}} \left(-\frac{2\pi y}{L}\hat{\mathbf{x}} + \frac{2\pi x}{L}\hat{\mathbf{y}} + \hat{\mathbf{z}} \right). \tag{9}$$

Taking the dot product of (8) and (9) to enforce $\mathbf{E} \cdot \hat{\mathbf{a}}_\parallel = 0$,

$$-\frac{2\pi y}{L} c_x(x) + \frac{2\pi x}{L} c_y(y) - \mu_0 \dot{H}_{a,x} y + \mu_0 \dot{H}_{a,y} x + c_z(z) = 0. \tag{10}$$

Rearranging,

$$y\left(-\frac{2\pi c_x(x)}{L\mu_0}-\dot{H}_{a,x}\right)+x\left(\frac{2\pi c_y(y)}{L\mu_0}+\dot{H}_{a,y}\right)+\frac{c_z(z)}{\mu_0}=0. \tag{11}$$

Setting the brackets that multiply x and y respectively to zero, we can find $c_x(x)$ and $c_y(y)$, and we can also set $c_z(z)=0$. Thus,

$$\mathbf{E}=\mu_0\left(-\dot{H}_{a,x}\frac{L}{2\pi}\hat{\mathbf{x}}-\dot{H}_{a,y}\frac{L}{2\pi}\hat{\mathbf{y}}+\left(\dot{H}_{a,y}x-\dot{H}_{a,x}y\right)\hat{\mathbf{z}}\right). \tag{12}$$

Note $\mathbf{J}_\perp=\frac{\mathbf{E}_\perp}{\rho_\perp}=\frac{\mathbf{E}}{\rho_\perp}$ because $\mathbf{E}$ has no component in $\hat{\mathbf{a}}_\parallel$.

The instantaneous power loss per unit volume (i.e. in W m^{-3}) of the filament-matrix zone due to the coupling current is

$$\begin{aligned}\frac{P_c}{V}&=\frac{1}{\pi R_\mathrm{f}^2}\iint_a \rho_\perp J_\perp^2\,\mathrm{d}a=\frac{1}{\pi R_\mathrm{f}^2\rho_\perp}\iint_a E^2\,\mathrm{d}a\\&=\frac{\mu_0^2}{\pi R_\mathrm{f}^2\rho_\perp}\iint_a\left(\dot{H}_{a,x}^2+\dot{H}_{a,y}^2\right)\left(\frac{L}{2\pi}\right)^2\\&\quad+\left(\dot{H}_{a,y}x-\dot{H}_{a,x}y\right)^2\mathrm{d}a\\&=\frac{\mu_0^2}{\pi R_\mathrm{f}^2\rho_\perp}\left(|\dot{\mathbf{H}}_\mathbf{a}|^2\left(\frac{L}{2\pi}\right)^2(\pi R_\mathrm{f})^2\right.\\&\quad\left.+\int_0^{R_\mathrm{f}}\int_0^{2\pi}\left(\dot{H}_{a,y}r\cos\theta-\dot{H}_{a,x}r\sin\theta\right)^2 r\,\mathrm{d}\theta\,\mathrm{d}r\right)\\&=\frac{\mu_0^2}{\pi R_\mathrm{f}^2\rho_\perp}\left(|\dot{\mathbf{H}}_\mathbf{a}|^2\left(\frac{L}{2\pi}\right)^2(\pi R_\mathrm{f})^2+\frac{R_\mathrm{f}^4}{4}\pi|\dot{\mathbf{H}}_\mathbf{a}|^2\right)\\&=\frac{|\dot{\mathbf{B}}_\mathbf{a}|^2}{\rho_\perp}\left(\frac{R_\mathrm{f}^2}{4}+\left(\frac{L}{2\pi}\right)^2\right),\end{aligned} \tag{13}$$

where a is the area of the filament-matrix zone, $|\dot{H}_\mathbf{a}|^2=|\dot{H}_{a,x}\hat{\mathbf{x}}+\dot{H}_{a,y}\hat{\mathbf{y}}|^2=(\dot{H}_{a,x})^2+(\dot{H}_{a,y})^2$, $\dot{\mathbf{B}}_\boldsymbol{a}=\mu_0\dot{\mathbf{H}}_\boldsymbol{a}$, $|\dot{\mathbf{B}}_\mathbf{a}|^2=(\dot{B}_{a,x})^2+(\dot{B}_{a,y})^2=\mu_0^2|\dot{\mathbf{H}}_\mathbf{a}|^2$.

The above expression agrees with [8, equation (9.4)] for the case when the external field is only in the x direction, i.e. $H_{a,y}=0$, and in such case, $|\dot{\mathbf{B}}_\mathbf{a}|^2=(\mu_0\dot{H}_{a,x})^2$.

2.2. Eddy current loss

In this subsection, we calculate the eddy current loss in the normal metal sheath surrounding the filament-matrix zone when a transverse field with components in both the x and y directions acts upon the wire. The method in [9] calculates the loss in the outer sheath when the wire is subject to a transverse field in one direction. Here, we adapt the method for a transverse field in two directions.

The local electric field in the sheath is [9]

$$\mathbf{E}=-\nabla V-\frac{\partial\mathbf{A}}{\partial t}, \tag{14}$$

where V is the electric scalar potential, $\mathbf{A}$ is the magnetic vector potential.

Taking the divergence of (14), $\nabla\cdot\nabla V=-\nabla\cdot\mathbf{E}-\frac{\partial}{\partial t}(\nabla\cdot\mathbf{A})$. Gauss's law gives $\nabla\cdot\mathbf{E}=\frac{\rho}{\epsilon_0}=0$ where there is no charge density (ρ is the charge density and ϵ_0 is the permittivity of free space). Under Coulomb's gauge, $\nabla\cdot\mathbf{A}=0$. Thus, we have the Laplacian of the electric scalar potential $\nabla\cdot\nabla V=0$. In 2D cylindrical coordinates (r,θ),

$$\frac{\partial^2V}{\partial r^2}+\frac{1}{r}\frac{\partial V}{\partial r}+\frac{1}{r^2}\frac{\partial^2V}{\partial\theta^2}=0. \tag{15}$$

To solve this Laplace's equation, we need two boundary conditions, at $r=R_\mathrm{f}$ and $r=R_0$.

In the filament-matrix zone, $\mathbf{E}$ is given in (12). As we assume full penetration of the external field[4], $\mathbf{B}=\mu_0(H_{a,x}\hat{\mathbf{x}}+H_{a,y}\hat{\mathbf{y}})$. With $\mathbf{B}=\nabla\times\mathbf{A}$, $\mathbf{A}=\mu_0(H_{a,x}y-H_{a,y}x)\hat{\mathbf{z}}$. Thus, (14) becomes

$$\begin{aligned}&\mu_0\left(-\dot{H}_{a,x}\frac{L}{2\pi}\hat{\mathbf{x}}-\dot{H}_{a,y}\frac{L}{2\pi}\hat{\mathbf{y}}+\left(\dot{H}_{a,y}x-\dot{H}_{a,x}y\right)\hat{\mathbf{z}}\right)\\&\quad=-\nabla V-\mu_0\left(\dot{H}_{a,x}y-\dot{H}_{a,y}x\right)\hat{\mathbf{z}}.\end{aligned} \tag{16}$$

The $\hat{\mathbf{z}}$ components cancel out[5]. Thus,

$$\begin{aligned}V&=\dot{B}_{a,x}\frac{L}{2\pi}x+\dot{B}_{a,y}\frac{L}{2\pi}y\\&=\dot{B}_{a,x}\frac{L}{2\pi}r\cos\theta+\dot{B}_{a,y}\frac{L}{2\pi}r\sin\theta.\end{aligned} \tag{17}$$

We can obtain the first boundary condition: in cylindrical coordinates and at $r=R_\mathrm{f}$

$$V=\frac{L}{2\pi}R_\mathrm{f}\left(\dot{B}_{a,x}\cos\theta+\dot{B}_{a,y}\sin\theta\right). \tag{18}$$

The second boundary condition is that at $r=R_0$, $E_r=-\frac{\partial V}{\partial r}=0$ [9].

The general solution to (15) is [20, chapter 34]

$$\begin{aligned}V(r,\theta)=a_0+b_0\ln r+\sum_{n=1}^{\infty}&\left[\left(a_nr^n+b_nr^{-n}\right)\cos(n\theta)\right.\\&\left.+\left(c_nr^n+d_nr^{-n}\right)\sin(n\theta)\right],\end{aligned} \tag{19}$$

where a_0,b_0,a_n,b_n,c_n,d_n are coefficients to be found based on boundary conditions.

[4] According to [9], the axial component of current density running through the filaments induced by an external magnetic field creates an additional homogeneous field in the opposite direction of the external field, giving a homogeneous internal total field. The internal field is assumed to be uniform and in the x direction [19]. Shielding due to the induced current is effective at $2\pi f\tau\gtrapprox 1$ where f is the frequency of the applied field, τ is the 'time constant governing the exponential decay of [the field generated by induced current]' [19]. However, we assume low external field frequency and thus assume full penetration, as used in [8, chapter 9.2] for a multifilament conductor without a sheath.

[5] In [9], it is assumed that $\frac{2\pi r}{L}<<1$, thus we can ignore E_z [9] (seen in (12)) and A_z.

Applying the first boundary condition (18), we obtain $a_0 = b_0 = 0$, $a_n = b_n = c_n = d_n = 0 \quad \forall n \neq 1$,

$$a_1 R_\mathrm{f} + \frac{b_1}{R_\mathrm{f}} = \frac{L}{2\pi}\dot{B}_{a,x} R_\mathrm{f} \tag{20}$$

$$c_1 R_\mathrm{f} + \frac{d_1}{R_\mathrm{f}} = \frac{L}{2\pi}\dot{B}_{a,y} R_\mathrm{f}. \tag{21}$$

For the second boundary condition on $r = R_0$, we obtain

$$0 = \frac{\partial V}{\partial r} = \left(a_1 - \frac{b_1}{r^2}\right)\cos\theta + \left(c_1 - \frac{d_1}{r^2}\right)\sin\theta. \tag{22}$$

Thus,

$$a_1 - \frac{b_1}{R_0^2} = 0 \tag{23}$$

$$c_1 - \frac{d_1}{R_0^2} = 0. \tag{24}$$

Solving for a_1, b_1, c_1, d_1, we get

$$V(r,\theta) = \frac{L}{2\pi}\frac{R_\mathrm{f}^2}{R_\mathrm{f}^2 + R_0^2}\left(r + \frac{R_0^2}{r}\right)\left(\dot{B}_{a,x}\cos\theta + \dot{B}_{a,y}\sin\theta\right). \tag{25}$$

With this expression of V, the components of $\mathbf{E}$ in the sheath are

$$\begin{aligned} E_r &= -\frac{\partial V}{\partial r} \\ &= -\frac{L}{2\pi}\frac{R_\mathrm{f}^2}{R_\mathrm{f}^2 + R_0^2}\left(1 - \frac{R_0^2}{r^2}\right)\left(\dot{B}_{a,x}\cos\theta + \dot{B}_{a,y}\sin\theta\right) \end{aligned} \tag{26}$$

$$\begin{aligned} E_\theta &= -\frac{1}{r}\frac{\partial V}{\partial \theta} \\ &= -\frac{L}{2\pi}\frac{R_\mathrm{f}^2}{R_\mathrm{f}^2 + R_0^2}\left(1 + \frac{R_0^2}{r^2}\right)\left(-\dot{B}_{a,x}\sin\theta + \dot{B}_{a,y}\cos\theta\right). \end{aligned} \tag{27}$$

Then,

$$\begin{aligned} E^2 &= E_r^2 + E_\theta^2 \\ &= \left(\frac{L}{2\pi}\frac{R_\mathrm{f}^2}{R_\mathrm{f}^2 + R_0^2}\right)^2 \left(\dot{B}_{a,x}^2\left[\left(1 + \frac{R_0^4}{r^2}\right) - \frac{2R_0^2}{r^2}\cos(2\theta)\right]\right. \\ &\quad + \dot{B}_{a,y}^2\left[\left(1 + \frac{R_0^4}{r^2}\right) + \frac{2R_0^2}{r^2}\cos(2\theta)\right] \\ &\quad \left. -4\dot{B}_{a,x}\dot{B}_{a,y}\sin(2\theta)\frac{R_0^2}{r^2}\right). \end{aligned} \tag{28}$$

where $\dot{B}_{a,x}^2 = \left(\dot{B}_{a,x}\right)^2$ and $\dot{B}_{a,y}^2 = \left(\dot{B}_{a,y}\right)^2$ for clarity. The power loss per unit of wire volume (i.e. in $\mathrm{W\,m^{-3}}$) is [9]

$$P_{ec} = \frac{1}{\pi R_0^2}\int_0^{2\pi}\int_{R_\mathrm{f}}^{R_0}\frac{E^2}{\rho_\mathrm{ms}} r\,\mathrm{d}r\,\mathrm{d}\theta, \tag{29}$$

which gives

$$P_{ec} = \left(\frac{R_\mathrm{f}}{R_0}\right)^2 \frac{1}{4\pi^2\rho_\mathrm{ms}}\left(\dot{B}_{a,x}^2 + \dot{B}_{a,y}^2\right)L^2\left(\frac{R_0^2 - R_\mathrm{f}^2}{R_\mathrm{f}^2 + R_0^2}\right), \tag{30}$$

where ρ_ms is the resistivity of the metal sheath. This agrees with [9, equation (13)] in the special case when the internal field has one direction only and is equal to the externally applied field $B(t) = B_{a,x}(t)\hat{\mathbf{x}}$.

2.3. Hysteresis loss

The hysteresis loss (per unit volume of a multifilament wire) of the superconducting filaments in a multifilament wire due to an external transverse magnetic field $\mathbf{H_a}$ can be calculated by λ times the expression of the hysteresis loss of a circular wire under the same transverse magnetic field of the same radius as the MgB_2 filament. This assumes that the field fully penetrates each filament and that the field acting on each filament is $\mathbf{H_a}$; that the filaments are circular; and that the external field is almost transverse to the filaments [8, p.127].

We now consider a circular MgB_2 filament (appendix C describes the loss of a hollow or composite MgB_2 filament) subject to the transverse external field $\mathbf{H_a}$. The transverse field required to fully penetrate a filament when there is no transport current is [8, equation (7.83)]

$$H_p = \frac{2}{\pi}R_\mathrm{fil}J_c, \tag{31}$$

where $R_\mathrm{fil} = d_\mathrm{fil}/2$ is the filament radius, d_fil is the filament diameter, and J_c is the critical current density of the filament. Suppose $d_\mathrm{fil} = 20 \times 10^{-6}$ m and $J_c = 2.81 \times 10^9\ \mathrm{A\,m^{-2}}$, then $H_p = 1.8 \times 10^4\ \mathrm{A\,m^{-1}}$, corresponding to the magnetic flux density of $H_p\mu_0 = 0.022$ T, which we assume will be exceeded in an electrical machine environment.

In the following, we modify [8, chapter 7.3], which calculates the hysteresis loss in a circular superconductor due to a transverse magnetising field in one direction that fully penetrates the superconductor when there is no transport current. Again, we consider a transverse field in two directions, $\mathbf{H_a} = H_{a,x}(t)\hat{\mathbf{x}} + H_{a,y}(t)\hat{\mathbf{y}}$.

Considering Faraday's law $\nabla \times \mathbf{E} = -\dot{\mathbf{B}}$, a general solution has already been given in (8). Suppose the solution to be

$$\mathbf{E} = \left(-\mu_0\dot{H}_{a,x}y + \mu_0\dot{H}_{a,y}x\right)\hat{\mathbf{z}}. \tag{32}$$

To check whether this is indeed the solution, inspired by [8, chapter 7.7, 7.11], we can observe that in this solution, $E = 0$ on the line $y = \frac{\dot{H}_{a,y}}{\dot{H}_{a,x}}x$, which passes through the origin (the centre of the wire), thus dividing the wire's cross section into two equal-area regions. Note, if $\mathbf{H_a}$ is a rotating field, the line with $E = 0$ rotates as well. As we adopt the critical state model when modelling the ac loss analytically, this means that both halves carry current densities J_c and $-J_c$, respectively ($E = 0$ is where the current density changes sign [8, p.90]), which matches the zero-transport current condition. Thus, (32) is an appropriate solution.

The instantaneous power loss per unit volume (in $\mathrm{W\,m^{-3}}$) of the circular superconductor with radius R_{fil} in a uniform magnetic field is [8, equation (7.1)]

$$\frac{P_{\mathrm{hys}}}{V} = \frac{1}{\pi R_{\mathrm{fil}}^2}\int_0^{2\pi}\int_0^{R_{\mathrm{fil}}} \mathbf{E}\cdot\mathbf{J} r\,\mathrm{d}r\,\mathrm{d}\theta. \tag{33}$$

Under the Bean critical state model assumptions, in areas of non-vanishing $\mathbf{E}$, the current density is in the direction of $\mathbf{E}$ and of magnitude J_c. Thus, assuming J_c is constant (independent of magnetic field), the hysteresis loss per unit of MgB_2 filament volume (in $\mathrm{W\,m^{-3}}$) is

$$\begin{aligned}\frac{P_{\mathrm{hys}}}{V} &= \frac{J_c}{\pi R_{\mathrm{fil}}^2}\int_0^{2\pi}\int_0^{R_{\mathrm{fil}}} E r\,\mathrm{d}r\,\mathrm{d}\theta \qquad (34)\\ &= \frac{J_c\mu_0}{\pi R_{\mathrm{fil}}^2}\int_0^{2\pi}\int_0^{R_{\mathrm{fil}}} |\dot{H}_{a,y}x - \dot{H}_{a,x}y| r\,\mathrm{d}r\,\mathrm{d}\theta\\ &= \frac{J_c\mu_0}{\pi R_{\mathrm{fil}}^2}\int_0^{2\pi}\int_0^{R_{\mathrm{fil}}} |\dot{H}_{a,y}\cos\theta - \dot{H}_{a,x}\sin\theta| r^2\,\mathrm{d}r\,\mathrm{d}\theta\\ &= \frac{J_c R_{\mathrm{fil}}}{3\pi}K \qquad (35)\end{aligned}$$

where

$$K = \mu_0\int_0^{2\pi} |\dot{H}_{a,y}\cos\theta - \dot{H}_{a,x}\sin\theta|\,\mathrm{d}\theta \tag{36}$$

$$= \begin{cases} 4\left(\dot{B}_{a,y}\sin\theta_1 + \dot{B}_{a,x}\cos\theta_1\right), & \text{if } \dot{B}_{a,x}\geqslant 0\\ -4\left(\dot{B}_{a,y}\sin\theta_1 + \dot{B}_{a,x}\cos\theta_1\right), & \text{if } \dot{B}_{a,x}<0\end{cases} \tag{37}$$

$$\theta_1 = \begin{cases} \tan^{-1}\left(\frac{\dot{B}_{a,y}}{\dot{B}_{a,x}}\right), & \text{if } \dot{B}_{a,x}\neq 0\\ \pi/2, & \text{if } \dot{B}_{a,x}=0, \dot{B}_{a,y}\geqslant 0\\ -\pi/2, & \text{if } \dot{B}_{a,x}=0, \dot{B}_{a,y}<0\end{cases} \tag{38}$$

$$\dot{B}_{a,x} = \mu_0\dot{H}_{a,x} \tag{39}$$

$$\dot{B}_{a,y} = \mu_0\dot{H}_{a,y}, \tag{40}$$

where $K, \theta_1, \dot{B}_{a,x}$ and $\dot{B}_{a,y}$ are all functions of time.

The above expression (35) agrees with [8, equation (7.26)] for the case when the transverse field is only in the x direction, i.e. $H_{a,y}=0$, giving $\frac{P_{\mathrm{hys}}}{V} = \mu_0\frac{4J_c}{3\pi}R_{\mathrm{fil}}|\dot{H}_{a,x}|$.

The hysteresis power loss per unit volume of the multifilament wire is (35) multiplied by the fill factor λ.

3. Numerical modelling

3.1. 3D model of homogenised filament-matrix zone plus outer sheath

This section follows [10] in implementing a 3D H-formulation anisotropic continuum model of a multifilament superconducting wire.

From Faraday's law,

$$\nabla\times\mathbf{E} = -\frac{\partial\mathbf{B}}{\partial t} = -\mu_0\mu_r\frac{\partial\mathbf{H}}{\partial t}, \tag{41}$$

where $\mathbf{E}$ is the electric field intensity, $\mathbf{B}$ is the magnetic flux density, $\mathbf{H}$ is the magnetic field strength, μ_0 is the permeability of vacuum, and μ_r is the relative permeability taken to be unity.

Substituting $\mathbf{E}=\boldsymbol{\rho}\mathbf{J}$ and $\mathbf{J}=\nabla\times\mathbf{H}$, where $\mathbf{J}$ is the current density and $\boldsymbol{\rho}$ is a resistivity matrix,

$$\nabla\times(\boldsymbol{\rho}\nabla\times\mathbf{H}) = -\mu_0\mu_r\frac{\partial\mathbf{H}}{\partial t}. \tag{42}$$

The condition $\nabla\cdot\mathbf{B}=0$ will hold for all time instants if the initial conditions satisfy [21]

$$\nabla\cdot(\mu_0\mu_r\mathbf{H})|_{t=0} = 0. \tag{43}$$

The outer sheath has an isotropic resistivity. The filament-matrix zone is homogenised according to the anisotropic continuum model, and the zone has an anisotropic resistivity, which is derived as follows (based on [10]).

To convert from cylindrical coordinates to Cartesian coordinates,

$$\hat{\mathbf{a}}_\theta = -\sin\theta\hat{\mathbf{x}} + \cos\theta\hat{\mathbf{y}} = -\frac{y}{r}\hat{\mathbf{x}} + \frac{x}{r}\hat{\mathbf{y}} \tag{44}$$

$$\hat{\mathbf{a}}_r = \cos\theta\hat{\mathbf{x}} + \sin\theta\hat{\mathbf{y}} = \frac{x}{r}\hat{\mathbf{x}} + \frac{y}{r}\hat{\mathbf{y}}. \tag{45}$$

Substituting the above into (2)–(4), the basis vectors in the helical coordinate system used in the anisotropic continuum model can be expressed in Cartesian coordinates:

$$\hat{\mathbf{a}}_1 = \hat{\mathbf{a}}_\parallel = -\frac{2\pi y/L}{k}\hat{\mathbf{x}} + \frac{2\pi x/L}{k}\hat{\mathbf{y}} + \frac{1}{k}\hat{\mathbf{z}} \tag{46}$$

$$\hat{\mathbf{a}}_2 = \frac{x}{r}\hat{\mathbf{x}} + \frac{y}{r}\hat{\mathbf{y}} \tag{47}$$

$$\hat{\mathbf{a}}_3 = -\frac{y/r}{k}\hat{\mathbf{x}} + \frac{x/r}{k}\hat{\mathbf{y}} - \frac{2\pi r/L}{k}\hat{\mathbf{z}}, \tag{48}$$

where $k=\sqrt{1+\left(\frac{2\pi r}{L}\right)^2}, r=\sqrt{x^2+y^2}$.

$\mathbf{J}$ and $\mathbf{E}$ can be expressed in Cartesian coordinates and helical coordinates:

$$\mathbf{J} = J_x\hat{\mathbf{x}} + J_y\hat{\mathbf{y}} + J_z\hat{\mathbf{z}} = J_1\hat{\mathbf{a}}_1 + J_2\hat{\mathbf{a}}_2 + J_3\hat{\mathbf{a}}_3 \tag{49}$$

$$\mathbf{E} = E_x\hat{\mathbf{x}} + E_y\hat{\mathbf{y}} + E_z\hat{\mathbf{z}} = E_1\hat{\mathbf{a}}_1 + E_2\hat{\mathbf{a}}_2 + E_3\hat{\mathbf{a}}_3. \tag{50}$$

Substituting (46)–(48) for $\hat{\mathbf{a}}_1, \hat{\mathbf{a}}_2$ and $\hat{\mathbf{a}}_3$, we obtain

$$\begin{bmatrix}J_x\\J_y\\J_z\end{bmatrix} = \begin{bmatrix}-\frac{2\pi y/L}{k} & \frac{x}{r} & -\frac{y/r}{k}\\ \frac{2\pi x/L}{k} & \frac{y}{r} & \frac{x/r}{k}\\ \frac{1}{k} & 0 & -\frac{2\pi r/L}{k}\end{bmatrix}\begin{bmatrix}J_1\\J_2\\J_3\end{bmatrix} = \mathbf{R}^{\mathsf{T}}\begin{bmatrix}J_1\\J_2\\J_3\end{bmatrix}, \tag{51}$$

$$\begin{bmatrix}E_x\\E_y\\E_z\end{bmatrix} = \mathbf{R}^{\mathsf{T}}\begin{bmatrix}E_1\\E_2\\E_3\end{bmatrix}, \tag{52}$$

where we have defined

$$\mathbf{R} = \begin{bmatrix} -\frac{2\pi y/L}{k} & \frac{2\pi x/L}{k} & \frac{1}{k} \\ \frac{x}{r} & \frac{y}{r} & 0 \\ -\frac{y/r}{k} & \frac{x/r}{k} & -\frac{2\pi r/L}{k} \end{bmatrix}. \tag{53}$$

Note $\mathbf{R}^\intercal = \mathbf{R}^{-1}$ because $\mathbf{R}$ is made of orthonormal vectors.

In the helical coordinate system $(\hat{\mathbf{a}}_1, \hat{\mathbf{a}}_2, \hat{\mathbf{a}}_3)$,

$$\begin{bmatrix} E_1 \\ E_2 \\ E_3 \end{bmatrix} = \begin{bmatrix} \rho_\mathrm{f} & 0 & 0 \\ 0 & \rho_\perp & 0 \\ 0 & 0 & \rho_\perp \end{bmatrix} \begin{bmatrix} J_1 \\ J_2 \\ J_3 \end{bmatrix}, \tag{54}$$

where the resistivity ρ_f along the filament direction follows the E–J power law:

$$\rho_\mathrm{f} = \frac{E_0}{J_c} \left(\frac{|J_\mathrm{f}|}{J_c} \right)^{n-1}, \tag{55}$$

where J_c is the critical current density of a filament and $J_\mathrm{f} = J_1$ is current density along the filament direction. The non-zero resistivity is in contrast to the analytical method in section 2.1, in which the electric field along the filament direction is assumed to be zero (i.e. $\rho_\mathrm{f} = 0$). A power-law resistivity is used in the 3D model in [10], and we do the same because of convergence difficulties in the 3D COMSOL model if $\rho_\mathrm{f} = 0$ is used. Nonetheless, $\rho_\mathrm{f} = 0$ is used for the 2D model described in section 3.2. However, as shown in section 4.1, there is little difference in the results between the 2D and 3D models under these assumptions.

Let us define

$$\boldsymbol{\rho}' = \begin{bmatrix} \rho_\mathrm{f} & 0 & 0 \\ 0 & \rho_\perp & 0 \\ 0 & 0 & \rho_\perp \end{bmatrix}. \tag{56}$$

Substituting (54) and (51) into (52),

$$\begin{bmatrix} E_x \\ E_y \\ E_z \end{bmatrix} = \mathbf{R}^\intercal \boldsymbol{\rho}' \begin{bmatrix} J_1 \\ J_2 \\ J_3 \end{bmatrix} = \mathbf{R}^\intercal \boldsymbol{\rho}' \mathbf{R} \begin{bmatrix} J_x \\ J_y \\ J_z \end{bmatrix}. \tag{57}$$

Thus, the anisotropic resistivity $\boldsymbol{\rho}$ is

$$\boldsymbol{\rho} = \mathbf{R}^\intercal \boldsymbol{\rho}' \mathbf{R}. \tag{58}$$

Note that this is similar to [10, 11] except that resistivity is used here, rather than conductivity.

In the COMSOL model, the H-formulation is implemented in the 'magnetic field formulation (mfh)' interface, which solves for the three Cartesian components of $\mathbf{H}$. Quadratic-order elements are used for better accuracy. $\mathbf{J}$ is calculated by implementing $\mathbf{J} = \nabla \times \mathbf{H}$,

$$J_x = \frac{\partial H_z}{\partial y} - \frac{\partial H_y}{\partial z} \tag{59}$$

$$J_y = \frac{\partial H_x}{\partial z} - \frac{\partial H_z}{\partial x} \tag{60}$$

$$J_z = \frac{\partial H_y}{\partial x} - \frac{\partial H_x}{\partial y}. \tag{61}$$

The resistivity tensor $\boldsymbol{\rho}$ is input as a user-defined resistivity in the E–J constitutive relation in the 'Faraday's Law' node of the mfh interface. The simulated geometry consists of a cylinder representing the filament-matrix zone enclosed by an outer cylinder representing the outer sheath, surrounded by a cylinder representing air (see figure 1(b)). One twist pitch is simulated. Periodic conditions are imposed at the two end faces of the 3D geometry[6].

The instantaneous coupling loss (in W) is calculated by integrating $E_2 J_2 + E_3 J_3$ over the filament-matrix zone volume. Note that there is J_1 in the filament direction, and since $E_1 = \rho_\mathrm{f} J_1$ is not zero, $E_1 J_1$ is not zero but is very small, as described in section 4.1. The instantaneous eddy current loss (in W) is calculated by integrating $E_x J_x + E_y J_y + E_z J_z$ over the sheath volume.

Compared to other numerical models for multifilament superconductors in which filaments are explicitly modelled and meshed, the anisotropic continuum model does not have individual filaments. The fill factor (proportion of superconductor filaments in the wire) probably affects the anisotropic continuum model via the transverse resistivity. Carr [8, chapter 8.5] suggests that the transverse conductivity depends on the conductivity of matrix σ_m, fill factor λ and filament-matrix interface resistance:

$$\sigma_\perp = \begin{cases} \sigma_m \frac{1+\lambda}{1-\lambda} & \text{, for no interface resistance} \\ \sigma_m \frac{1-\lambda}{1+\lambda} & \text{, for large interface resistance} \end{cases}. \tag{62}$$

In the future, comparisons can be made between the anisotropic continuum model and models that model filaments explicitly.

3.2. 2D model of homogenised filament-matrix zone plus outer sheath

The analytical calculation in (13) of the coupling loss of the filament-matrix zone given by the anisotropic continuum model has no dependence on z. The anisotropic resistivity in (58) also has no dependence on z, despite the fact that in a real wire, the cross-section changes with z as the filaments are twisted. Thus, the anisotropic continuum model is also implemented in a 2D geometry in COMSOL assuming electromagnetic quantities do not change with z.

The 2D geometry in COMSOL representing the cross-section of the wire is shown in figure 1(b). The geometry consists of three concentric circles, representing the filament-matrix zone, the outer sheath, and air, respectively. Under the

[6] (In COMSOL 6.2) Periodic conditions imposed by first adding a 'Linear Extrusion' node (suppose the operator name is 'linext1') under 'Definitions' to select the source nodes on the source face and corresponding destination nodes on the destination face, and then adding a 'Magnetic Field' node in the mfh module with the destination face selected and imposing the magnetic field as 'linext1(Hx)' for the x component of $\mathbf{H}_0$ and so on.

mfh node, the 'field components solved for' is set to be the 'three-component magnetic field' option, so that all three components of $\mathbf{H}$ are solved. The three components of $\mathbf{J} = \nabla \times \mathbf{H}$ are calculated as

$$J_x = \frac{\partial H_z}{\partial y} \tag{63}$$

$$J_y = -\frac{\partial H_z}{\partial x} \tag{64}$$

$$J_z = \frac{\partial H_y}{\partial x} - \frac{\partial H_x}{\partial y}, \tag{65}$$

since $\frac{\partial H_x}{\partial z}$ and $\frac{\partial H_y}{\partial z}$ are assumed to be zero as the 2D model assumes electromagnetic quantities have no z dependence. The 3-by-3 resistivity tensor $\boldsymbol{\rho}$ is input as the user-defined resistivity in the E–J constitutive relation in the 'Faraday's Law' node of the mfh interface. Note that we implement $\rho_{\mathrm{f}} = 0$ for (56) in the 2D model.

The instantaneous coupling loss (in $\mathrm{W\,m^{-1}}$) is calculated by integrating $E_2 J_2 + E_3 J_3$ over the filament-matrix zone area. Note that $E_1 J_1 = 0$ because $\rho_{\mathrm{f}} = 0$. The instantaneous eddy current loss (in $\mathrm{W\,m^{-1}}$) is calculated by integrating $E_x J_x + E_y J_y + E_z J_z$ over the sheath area.

3.3. 2D model of single circular superconductor

To model an untwisted superconducting circular filament in isolation in air in 2D, the QCSM in [22] is used, where

$$J_z = J_c \operatorname{erf}\left(\frac{E_z}{E_0}\right) \tag{66}$$

where $\operatorname{erf}(x)$ is the error function [23], which transitions smoothly from -1 to 1 as the argument x changes from negative to positive (the transition is almost complete over an interval of approximately $-2 < x < 2$), thus J_z as a function of E_z resembles a smoothed version of the critical state model. This is implemented in the 'magnetic fields (mf)' interface in COMSOL (which solves the magnetic vector potential) by setting the isotropic electrical conductivity in the superconductor region to be

$$\sigma = \frac{J_c \operatorname{erf}(E_z/E_0)}{|E_z + \epsilon|}, \tag{67}$$

where ϵ is a small constant ('eps' in COMSOL) to avoid a singularity.

Only the out-of-plane vector potential is solved for in the mf interface, and thus $J_x = J_y = 0$. The instantaneous hysteresis per unit length (in $\mathrm{W\,m^{-1}}$) is calculated by integrating $E_z J_z$ over the filament area.

4. Results

In this section, let us consider the magnetic field experienced by a wire in the armature of a superconducting machine. A general synchronous machine is shown in figure 3 with two pole pairs. We consider a dc synchronous machine with four pole pairs of ratings 3 MW, 4500 rpm, which correspond to ratings for NASA's N3-X concept plane [24]. For such a

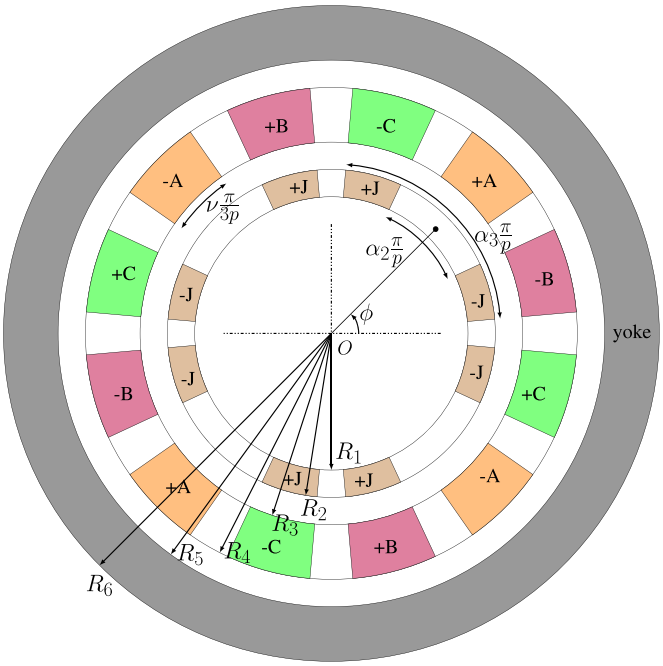

Figure 3. The synchronous machine that generates the magnetic field considered in section 4. Adapted with permission from [44], which is © [2025] IEEE.

machine, the magnetic flux density in two directions, B_r and B_θ, experienced at a point in the armature coil area is evaluated at discrete time instants and is given in figures 4(a) and (b), respectively. The evaluation is carried out in Python and is based on a 2D analytical model [25] to model magnetic field in the machine. Using a fast Fourier transform, the frequency components of B_r and B_θ are identified, and time-continuous signals based on the four harmonics with the largest amplitudes are constructed for each of B_r and B_θ, shown as solid lines in figure 4(b). For the simulations in this section, the external field experienced by an MgB_2 wire is based on these time-continuous signals:

$$B_r = \sum_{n=1,3,5,7} a_n \cos\left(2\pi\ (300)\, nt + \alpha_n\right) \tag{68}$$

$$B_\theta = \sum_{n=1,3,5,7} b_n \cos\left(2\pi\ (300)\, nt + \beta_n\right), \tag{69}$$

where the coefficients are detailed in table 1.

4.1. Instantaneous power dissipation due to coupling and eddy current losses

Consider a wire of length L specified in table 2 subject to a transverse magnetic field in the x and y directions like (68) and (69), respectively, but multiplied by a ramp function $r(x) = 1/(1 + \exp(-5(10x - 1.8)))$ to allow zero initial conditions for ease of simulation,

$$B_x = r(300t) \sum_{n=1,3,5,7} a_n \cos\left(2\pi\ (300)\, nt + \alpha_n\right) \tag{70}$$

$$B_y = r(300t) \sum_{n=1,3,5,7} b_n \cos\left(2\pi\ (300)\, nt + \beta_n\right). \tag{71}$$

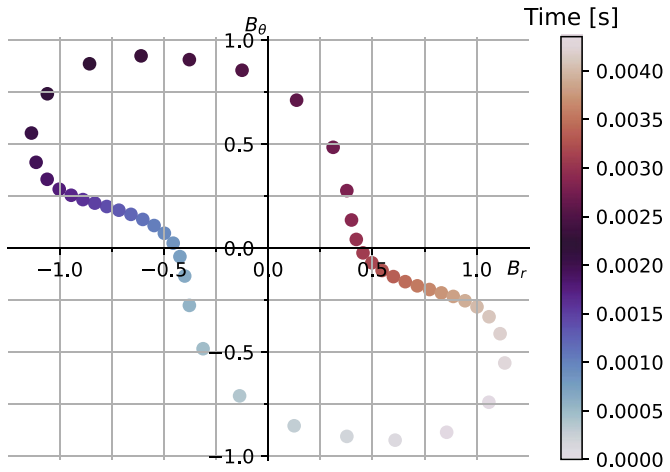

(a)

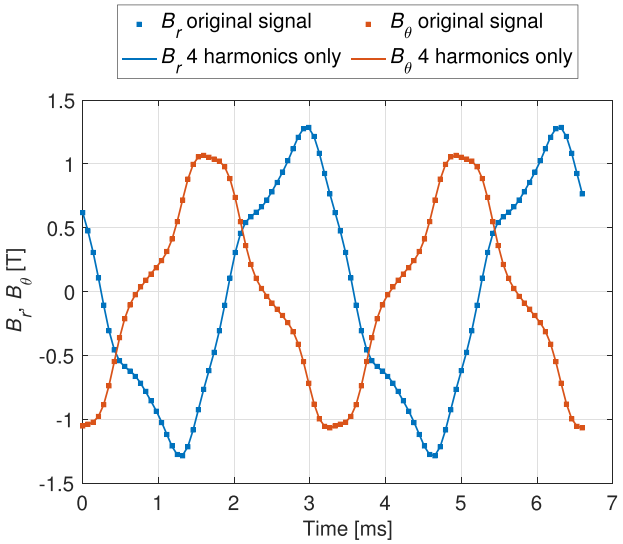

(b)

Figure 4. The magnetic flux density in radial and tangential directions at a point in the armature of a synchronous machine, evaluated at different time instants, presented as (a) a scatter plot for one electrical period, with each dot separated by a fixed time interval, (b) time series for two electrical periods. In (b), the original time-discretised B_r and B_θ signals are analysed by a fast Fourier transform and time-continuous signals are reconstructed based on the four harmonics with the largest amplitudes for each signal.

Table 1. Amplitude and phase of harmonics in B_r and B_θ.

Amplitude	Value [T]	Phase	Value [rad]
a_1	1.1524	α_1	1.0086
a_3	0.1810	α_3	1.3996
a_5	0.0429	α_5	−1.8562
a_7	0.0326	α_7	−1.9703
b_1	0.9448	β_1	−3.0817
b_3	0.1810	β_3	2.9704
b_5	0.0429	β_5	−0.2854
b_7	0.0326	β_7	−0.3995

The wire is simulated for two periods $(2/f)$, where $f = 300$ Hz, in 2D and 3D in COMSOL according to sections 3.2 and 3.1, respectively. The simulated 2D and 3D geometries are shown in figures 1(a) and (b), respectively. The 2D and 3D models have the same mesh settings (maximum size and so on) for the cross-section (the 3D model has a swept mesh

Table 2. MgB_2 wire parameters

Description	Symbol	Unit	Value
Radius of filament-matrix zone	R_f	m	240×10^{-6}
Outer radius of outer sheath	R_0	m	305×10^{-6}
Twist pitch	L	m	5×10^{-3}
Transverse resistivity of filament-matrix zone	$\rho_\perp$	Ωm	5×10^{-8}
Resistivity of outer sheath	ρ_{ms}	Ωm	365×10^{-9}
MgB_2 filament diameter (for hysteresis loss formula and simulation involving one filament)	d_{fil}	m	20×10^{-6}
For COMSOL simulation (for (55) and (67))			
n value in E–J power law	n	—	42
Filament critical current density	J_c	$A\,m^{-2}$	2.81×10^9
Critical electric field[a]	E_0	$V\,m^{-1}$	10^{-5}

R_f, R_0, L, ρ_{ms}, and λ are taken from [26, tables 2.1, 2.2]; the value for $\rho_\perp$ is within the range given in [6, table 5]. n and E_0 are taken from table 1 in [10], which are for LTS, but we use them here nevertheless. J_c for MgB_2 filament is reasonable from figure 6 of [27].
[a] A comparison between COMSOL simulations with $E_0 = 10^{-5}\ V\,m^{-1}$ and $E_0 = 10^{-4}\ V\,m^{-1}$ is provided in appendix D.

and thus the mesh on one of the 2D faces is specified), but the resulting meshes are not exactly the same.

The instantaneous loss results calculated by the COMSOL simulations and analytical method (in section 2.1 for coupling loss and section 2.2 for eddy current loss) are given in figures 5(a) and (b). As with all loss simulations in this paper, two periods are simulated and results at 401 evenly distributed time steps are stored. Analytical instantaneous loss formulae are also evaluated at the same 401 time steps. In 3D, one twist pitch is simulated; and in 2D, the instantaneous loss result (in $W\,m^{-1}$) is multiplied by the twist pitch to give the unit of watt. The average loss values and time taken for the simulations are given in table 3. Very good agreement can be seen between 2D and 3D simulations. Furthermore, the difference between the average loss values from the analytical calculations are within 4% of the simulated value (2D) for coupling loss and 7.5% of the simulated value (2D) for eddy current loss.

Although non-zero resistivity (power-law resistivity) is used in the 3D model along the filament direction $\hat{\mathbf{a}}_1$, the loss in that direction is very small: integrating $E_1 J_1$ over the filament-matrix zone volume and averaging over the second period simulated gives only 11.4 μW, which is very small compared to the mW level of coupling and eddy current losses in table 3.

4.2. Instantaneous power dissipation due to hysteresis loss

Consider a straight and untwisted circular MgB_2 filament in air in isolation with J_c and diameter in table 2. It is subject to a transverse magnetic field (with harmonics) in the x and y directions, with B_x and B_y given by (70) and (71), respectively.

The hysteresis loss of the wire is calculated by the analytical method in section 2.3, and by the 2D model in COMSOL described in section 3.3 using the parameters in table 2. Two periods $(2/f)$, where $f = 300$ Hz, are simulated. The results are shown in figure 6, and there is very good agreement between the two methods. The average loss over the second period calculated by the analytical method and by the COMSOL simulation are 8.2339 mW and 8.2308 mW, respectively, showing a difference of less than 0.04%. The time taken by COMSOL simulation is 1881 s. The time taken by the analytical method is very fast (less than 1 s in Matlab, but the analytical formula is also implemented in COMSOL, from which analytical instantaneous loss values are obtained).

4.3. Average losses as magnetic field amplitude varies

Consider a wire of length L specified in table 2 subject to a transverse magnetic field in the x and y directions,

$$B_x = kr(300t) \sum_{n=1,3,5,7} a_n \cos(2\pi\,(300)\,nt + \alpha_n) \tag{72}$$

$$B_y = kr(300t) \sum_{n=1,3,5,7} b_n \cos(2\pi\,(300)\,nt + \beta_n), \tag{73}$$

where k is an amplitude factor that is varied from 0.002 to 20. When $k = 1$, the amplitude of the external magnetic field is approximately 1.5 T. The wire is simulated for two periods $(2/f)$, where $f = 300$ Hz, in 2D. The average coupling loss and eddy current loss over the second period calculated in COMSOL are compared to the analytical calculations from the formulae in section 2.1 for coupling loss and section 2.2 for eddy current loss. The results are shown in figure 7. It can be seen that the analytical formulae agree with the 2D numerical simulations for the wide range of amplitudes simulated (difference within 4.6% for the coupling loss and 7.5% for the eddy current loss).

Next, for hysteresis loss, we simulate in COMSOL an MgB_2 filament subject to the same transverse magnetic field in the x and y directions in (72) and (73), respectively, except that k varies from 0.001 to 10. The filament is simulated for two periods $(2/f)$, $f = 300$ Hz. The average power dissipation per meter over the second period calculated in COMSOL is compared to the analytical calculation from the formulae

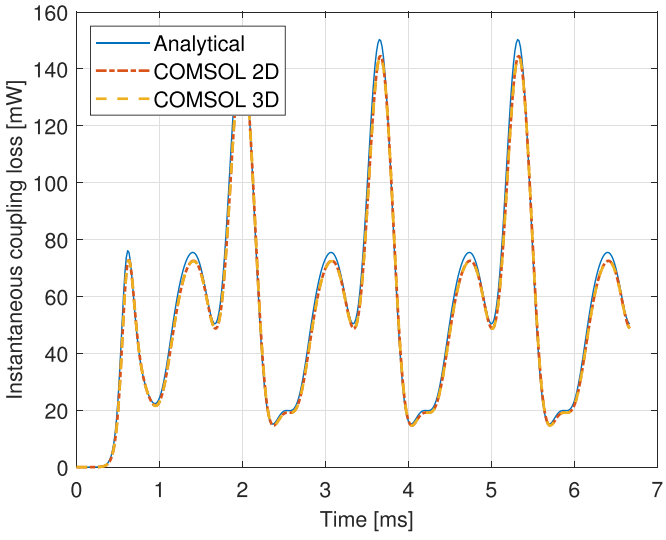

(a)

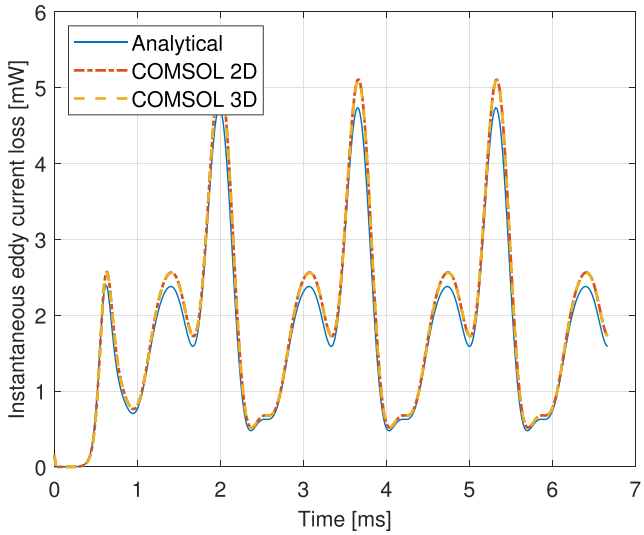

(b)

Figure 5. Instantaneous (a) coupling loss and (b) eddy current loss calculated by the analytical method, and 2D and 3D COMSOL simulations, over two periods.

Table 3. Coupling loss and eddy current loss simulation results.

		COMSOL	
Description	Analytical	2D	3D
Average[a] coupling loss in filament-matrix zone [mW]	62.598	60.286	60.185
Average[a] eddy current loss in sheath [mW]	1.9719	2.1305	2.1251
Time taken for simulation[b] [s]	<1	146	16 952

[a] Averaged over the second period simulated.
[b] Time for analytical calculation is based on implementation in Matlab, but analytical calculations are also performed in COMSOL, from which we take the analytical average loss values and instantaneous loss values for plotting in figures.

in section 2.3. The results are shown in figure 7. It can be seen that for $k < 0.1$, there starts to be significant differences between numerical and analytical methods. This is reasonable because, as stated in (31), the hysteresis loss formula is only valid if the external magnetic field fully penetrates the filament (the penetration field is calculated to be 0.022 T) and it is

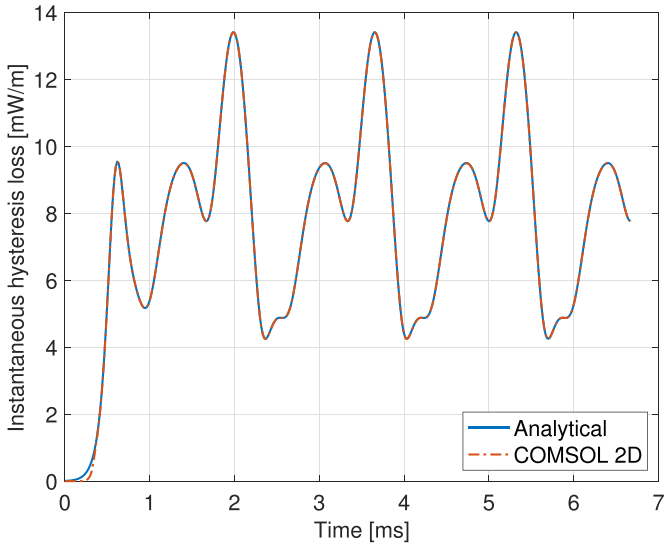

Figure 6. Instantaneous hysteresis loss of a circular MgB_2 filament in air in isolation, calculated by analytical means and a 2D COMSOL simulation.

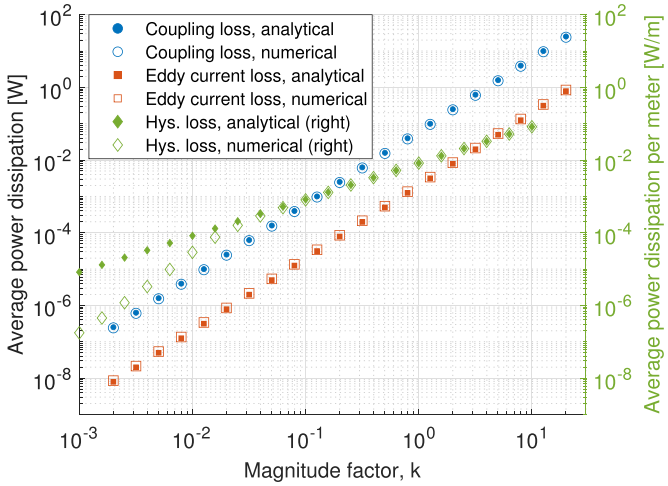

Figure 7. Average power dissipation of a multifilament wire due to coupling and eddy current losses (left axes) and average power dissipation per meter of an MgB_2 filament due to hysteresis loss (right axes) as the amplitude of the external magnetic field is varied.

assumed in the derivation of the hysteresis loss formula that the external field is equal to the field in the filament. Thus, at $k = 0.1$, the external field has amplitude 0.15 T, which ensures that the external field fully penetrates the filament and that the induced current in filaments does not alter the magnetic field inside the filament much (such that the magnetic field inside the filament is more or less the same as the external magnetic field). The analytical hysteresis loss results are within 3% of the numerical results for $k \geqslant 0.1$, and within 0.04% for $k \geqslant 1$.

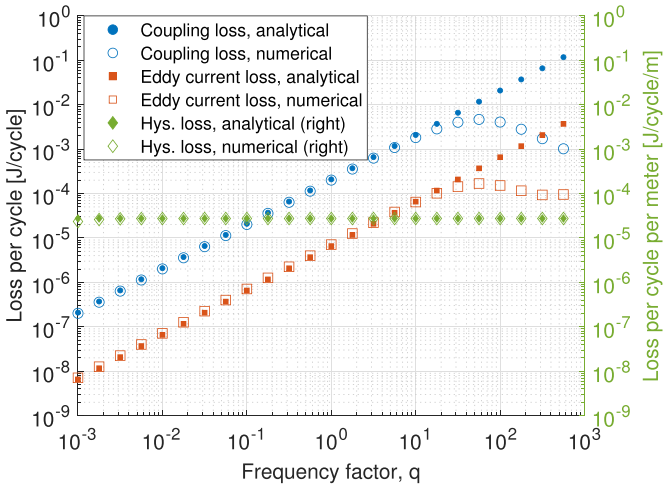

Figure 8. Energy loss per cycle of a multifilament wire of length L due to coupling and eddy current losses (left axes) and energy loss per cycle per meter of an MgB_2 filament due to hysteresis loss (right axes) as the frequency of the external magnetic field is varied.

4.4. Average losses as frequency of magnetic field varies

Consider a wire of length L specified in table 2 subject to a transverse magnetic field in the x and y directions,

$$B_x = r(300qt) \sum_{n=1,3,5,7} a_n \cos\left(2\pi\ (300)\, qnt + \alpha_n\right) \qquad (74)$$

$$B_y = r(300qt) \sum_{n=1,3,5,7} b_n \cos\left(2\pi\ (300)\, qnt + \beta_n\right), \qquad (75)$$

where q is a frequency factor that is varied from 0.002 to 20. When $q = 1$, the fundamental frequency of the magnetic field variation is 300 Hz. The wire is simulated for two periods $(2/f)$, where $f = 300q$ Hz, in 2D. The average coupling loss and eddy current loss over the second period calculated in COMSOL are compared to the analytical calculations. The results are shown in figure 8. It can be seen that the numerical and analytical results agree reasonably below $q = 10$ (difference within 15% for the coupling loss and 8% for the eddy current loss if $q \leqslant 10$). However, the numerical and analytical results begin to deviate significantly for $q > 10$. The reason for this is that, as indicated by (6), the coupling loss formula is only valid when the external field is below a certain frequency such that it varies slowly enough not to cause the interior to be shielded, and we calculated that such shielding occurs at around $f_1 = 20$ kHz. At $q = 10$, the fundamental frequency of the external magnetic field is 3 kHz, but there are also higher harmonics in the external magnetic field. To learn more about the difference between analytical and numerical methods as the frequency approaches f_1, we calculate the coupling and eddy current losses of the wire when the external field is without harmonics: $B_x = r(ft)a_1 \cos(2\pi ft + \alpha_1)$ and $B_y = r(ft)b_1 \cos(2\pi ft + \beta_1)$, and we vary the frequency f. The results are shown in figure 9. We see that the deviation becomes significant at $f_1 = 20$ kHz.

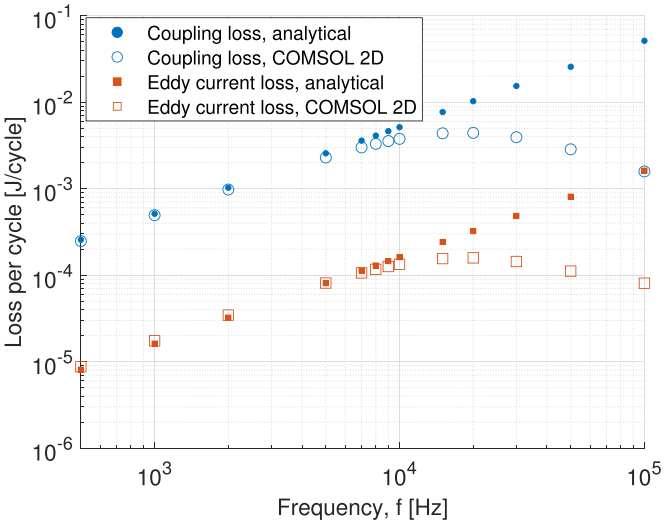

Figure 9. Coupling and eddy current losses per cycle of a multifilament wire of length L due to a single-tone external field in two directions as the frequency of the external magnetic field is varied.

Next, for hysteresis loss, we simulate in COMSOL an MgB_2 filament subject to the same transverse magnetic field in the x and y directions as (74) and (75), respectively. The filament is simulated for two periods $(2/f)$, where $f = 300q$ Hz. The energy loss per meter over the second period calculated in COMSOL is compared to the analytical calculation. The results are shown in figure 8. It can be seen that numerical and analytical results generally agree well with each other, which is expected as hysteresis loss should not depend on frequency. The analytical hysteresis loss results are within 0.25% of the numerical results for $q \geqslant 0.01$.

5. Discussion

This section discusses reasons for the discrepancy between the analytical and numerical calculations of the coupling and eddy current losses when we expect the analytical formulae to be valid.

One reason could be that in the analytical calculations for the coupling and eddy current losses, the magnetic field inside the filament-matrix zone and sheath is assumed to be the same as the external field (full penetration assumed). However, the magnetic field generated by the induced current is not considered.

For the eddy current loss, the boundary conditions of the sheath in COMSOL are not exactly the same as in the theory. From section 2.2, E_r at the outer radius of the sheath is supposed to be 0. E_r at the inner sheath radius is supposed to be $E_r = -\frac{\partial V}{\partial r}$ with V in (17), i.e.

$$E_r = -\frac{L}{2\pi}\left(\dot{B}_{a,x}\cos\theta + \dot{B}_{a,y}\sin\theta\right). \tag{76}$$

For B_x and B_y in (70) and (71), respectively, at the end of the second period at $t = 2/f$, where $f = 300$ Hz, the theoretical E_r at the inner radius according to (76) is shown in figure 10(a),

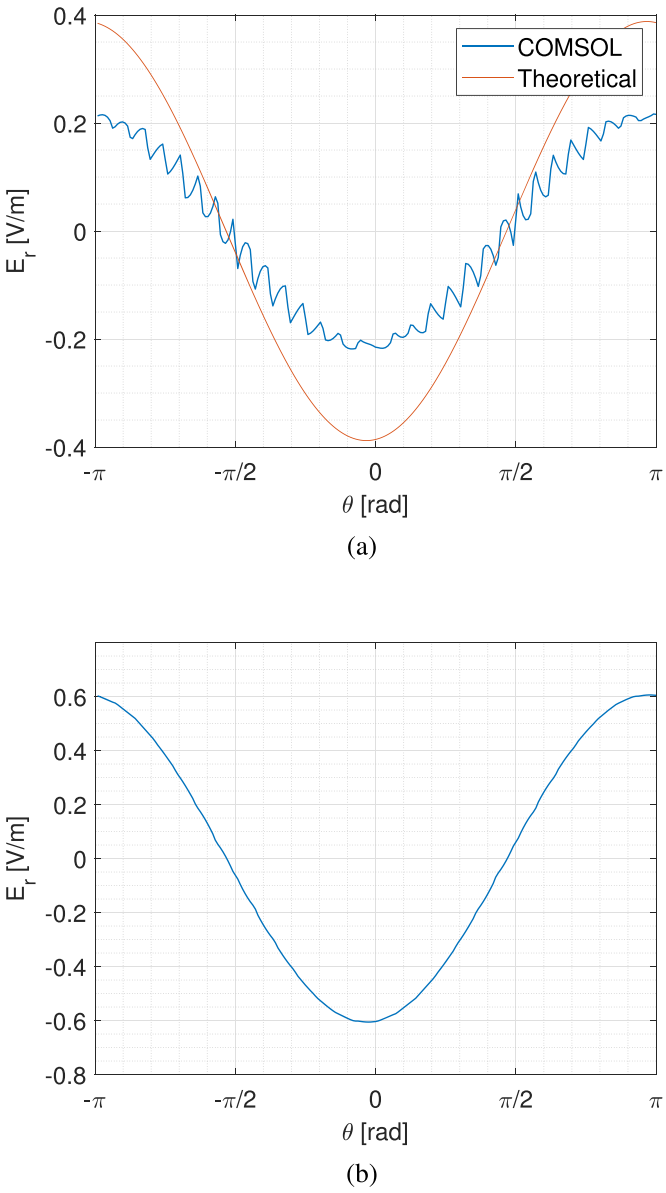

Figure 10. The value of E_r at the (a) inner and (b) outer radii of the sheath in the COMSOL simulation at the end of the second period.

with amplitude of approximately 0.4 V m^{-1}. However, the value of E_r at the inner and outer radii of the sheath in the COMSOL simulation at the end of the second period is shown in figures 10(a) and (b), respectively. The values are different from what is predicted in the analytical calculation. At the inner radius, the amplitude of E_r is only 0.2 V m^{-1}, which is lower than the 0.4 V m^{-1} predicted. At the outer radius, the amplitude is not 0 V m^{-1} as expected. To get a better understanding, we also plot E_r of the conductor and surrounding air region at the end of the second period in figure 11. E_r at the outer radius of the sheath is also not zero and this could be due to the presence of air (which is modelled as a non-zero resistivity in the H-formulation in COMSOL).

We tried to improve the model by increasing the mesh density of the filament-matrix zone and sheath area and removing the air region and setting the magnetic field at the outer radius

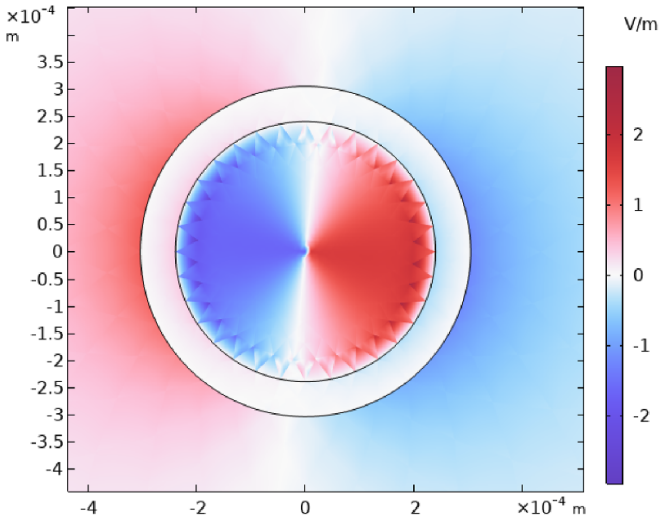

Figure 11. E_r of the multifilament wire under an external magnetic field of (70) and (71) at $t = 2/f, f = 300$ Hz., simulated in a 2D COMSOL model.

of the sheath to be the applied field. This makes E_r at the outer radius of the sheath much closer to 0, but E_r at the inner radius still has an amplitude of approximately 0.2 V m^{-1}. In that case, the average coupling loss (at 61.456 W) moves closer to the analytically calculated value in table 3, but the eddy current loss (at 2.2095 W) moves further away from the analytically calculated value.

6. Conclusion

This paper has made two main contributions. First, we show that the anisotropic continuum model can be implemented in both 2D and 3D in COMSOL, whereas the literature has implemented the anisotropic continuum model in COMSOL in 3D only (a 2D model has been implemented in another computer program [11]). The 2D model is much faster than the 3D model, but the results are very similar.

Second, we derive analytical magnetisation formulae for a multifilament (MgB_2 or low-temperature superconductors like NbTi or Nb_3Sn) superconducting wire under a time-varying external magnetic field with two orthogonal components transverse to the wire axis. The instantaneous coupling loss, eddy current loss, and hysteresis loss are calculated. The analytical formulae are much faster than numerical simulations, and they are verified by comparing analytical results with numerical ones for external field conditions that are realistic in an electrical machine. In the results section, we highlight the importance of using these formulae within their valid range: the coupling and eddy current loss formulae are valid when the frequency of the external field is low enough not to cause shielding; the hysteresis formula is valid when the amplitude of the external field is high enough for full penetration of the filament. Although there are some differences between numerical and analytical results, the errors may be acceptable at the initial machine design stage, and precise estimations can be made with numerical models.

In the future, a comparison can be made between the anisotropic continuum model and other models to calculate ac loss of MgB_2 wires, and with experimental methods. In addition, this study does not consider the effect of transport current, which MgB_2 wires would carry in an electrical machine. The effect of transport current is an important topic for future study.

Data availability statement

COMSOL files run into GB in size and are not easily deposited. The data that support the findings of this study are available upon reasonable request from the authors.

Acknowledgments

This work was supported in part by the Hong Kong Research Grants Council, Hong Kong Special Administrative Region, China, under Project No. 17204021, and in part by The Hong Kong Polytechnic University, Hong Kong Special Administrative Region, China, under Project Nos. P0048560 and P0046563.

Parts of this paper appear in the PhD thesis of CCT Chow.

Appendix A. Comment on calculating total ac loss of MgB_2 wires in a machine

It is typical in the literature to calculate the magnetisation losses and transport losses separately if the losses are to be calculated analytically, for example, as done in [1, 28–30]. Nonetheless, Terao *et al* [31] used this simple summation method and compared the results obtained with experimental results for an MgB_2 coil subject to an external magnetic field (due to rotating magnets) whilst simultaneously carrying transport ac current (induced by the rotating field due to the rotating magnets as the coil operated under generator mode). Good agreement between analytical predictions and experimental results was found. Coupling loss was found to be the dominant loss, and transport ac loss was calculated to be small. Furthermore, a very recent paper [45] shows in numerical simulations that the total loss for a multifilament MgB_2 wire under simutaneous application of transport ac current and time-varying external magnetic field is the sum of transport losses and magnetisation losses.

Theoretical formulae are available in the literature for loss in a superconducting filament for the simple case of sinusoidal transport ac current in phase with sinusoidal external magnetic field [26, section 2.3.1][8, section 7.9] [32, section 4.3.4]. Modifications to calculate loss under non-sinusoidal magnetic field with two orthogonal components plus transport ac current can be a topic of future research but is beyond the scope of this paper.

Appendix B. Note on practical MgB_2 wires

MgB_2 wires are widely made via one of the two processes: powder-in-tube (PIT) and internal Mg diffusion

(IMD). PIT is the more popular option and PIT wires are available commercially, whereas IMD wires are not available commercially [26].

B.1. Powder-in-tube (PIT) wires

The PIT method can further be divided into *in situ* or *ex situ* methods. In the *in situ* method, unreacted Mg and B powders are packed into a metal tube, which (combined with other similar tubes if a multifilament MgB_2 wire is desired) is rolled and deformed into a wire, and then goes through heat treatment to react the powders. In the *ex situ* method, reacted MgB_2 powder is packed into metal tube(s), which is then drawn into a wire and undergoes heat treatment. During the production of *in situ* wires, reaction between Mg and B leads to volume shrinkage (since MgB_2 has a higher density than Mg and B), leading to voids forming and a porous MgB_2 layer, resulting in low critical current density [33]. On the other hand, *ex situ* PIT also has low critical current density, because MgB_2 has low connectivity as MgB_2 is a hard ceramic [33].

MgB_2 filaments made from the *in situ* method have a fibrous structure, due to elongation of Mg powder during wire drawing before heat treatment [34, 35]. The relationship between microstructure (or 'macrostructure' as used in [35] to describe the structure of filaments, which are much larger than MgB_2 grains) and critical current density, and factors affecting the microstructure, have been explored in the literature. For example, the effect of heat treatment on the morphology and critical current density of MgB_2 wires with addition of Sm_2O_3 dopant was investigated in [36]; the formation of uniform and homogeneous structure without any voids when reacting MgB_2 under pressure was reported in [37]; and production of wires suitable for ITER applications that used MgB_2 made from isotope ^{11}B was reported in [38].

In this paper, microstructure has not been considered explicitly but is taken into account by the critical current density of the filament, which is used to calculate the hysteresis loss. Although the fibrous structure leads to anisotropic critical current density [35], the critical current density used in this paper is the critical current density in the longitudinal direction of the filament rather than that in the transverse direction, since the transverse magnetic field applied leads to current in the longitudinal direction.

B.2. Internal magnesium diffusion (IMD) wires

In the IMD method [39–41], a pure Mg rod is inserted into a metal tube (Fe or Nb or Ti, with a possible outer Cu or Monel layer), and B powder fills the space between the Mg tube and the outer metal tube. The composite wire is cold drawn into the desired shape, and then goes through heat treatment, during which Mg diffuses and reacts with B to produce a dense MgB_2 layer, leaving behind an empty cylinder where the Mg rod was, thus the MgB_2 layer is more like an annulus rather than a cylinder. The annulus geometry of a filament may affect the calculation for hysteresis loss, which in the main text is presented for a cylindrical filament. However, [42] substituted the central Mg rod with Mg powder, and Mg/B pellets with excess Mg, respectively; thus instead of leaving a central void as in traditional IMD, a central porous MgB_2 structure was left at the centre surrounded by the dense MgB_2 layer seen in typical IMD wires.

Coupling loss formulae developed should be valid for multifilament IMD wires regardless of the detailed geometry of the filaments because a homogenised model is used, and the loss is due to current in the matrix (current in the filaments assumed to be lossless). Since the majority of the loss is coupling loss (in our analysis with cylindrical filaments), our analysis can still be useful for multifilament MgB_2 wires made from the IMD process, as the coupling loss formulae should still be valid.

Our hysteresis loss formulae may be affected because the each filament is no longer a cylinder but more like an annulus. Thus, hysteresis loss formulae for such geometry are provided in appendix C.

Appendix C. Hysteresis loss of filament made of two concentric cylinders of different superconductors

The hysteresis loss of a composite superconductor consisting of an inner cylinder of one type of superconductor (of critical current J_{c2}) inside an outer cylinder of another type of superconductor (of critical current J_{c1}) is now considered. The instantaneous hysteresis loss due to an external transverse field in one direction for such a conductor has been calculated in [8], and here we extend the method to an external transverse field in two directions based on [8]. The procedure is very similar to section 2.3.

Suppose the external field is much larger than the field needed to fully penetrate the composite filament, which is [8, equation (7.79)]

$$H_p = \frac{2}{\pi}\left((R_{\rm fil} - R_i)J_{c1} + R_i J_{c2}\right), \tag{C1}$$

where $R_{\rm fil}$ is radius of the outer cylinder, and R_i is radius of the inner cylinder.

Table C1. Composite filament parameters for appendix C.

Parameter	Sym.	Unit	Case 1	Case 2
Radius of inner cylinder[a]	R_i	μm	40	40
Radius of outer cylinder[a]	R_{fil}	μm	50	50
Critical current density of inner cylinder	J_{c2}	A m^{-2}	0	3×10^9
Critical current density of outer cylinder[b]	J_{c1}	A m^{-2}	9×10^9	9×10^9
Critical electric field	E_0	V m^{-1}	10^{-5}	10^{-5}
Average[c] hysteresis loss calculated by analytical means	—	W	8.0459	10.860
Average[c] hysteresis loss calculated by COMSOL	—	W	8.0393	10.846

[a] Based on the rough geometry of a filament in the multifilament MgB_2 wire B1 fabricated by the IMD technique in [43, section 3.2].
[b] Based on layer J_c of IMD MgB_2 at 2 T, 4.2 K reported in [43, figure 5].
[c] Averaged over the second period simulated.

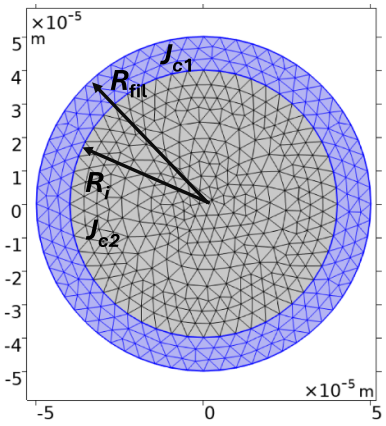

Figure C1. Geometry of a composite filament made of two concentric circles of different superconductors.

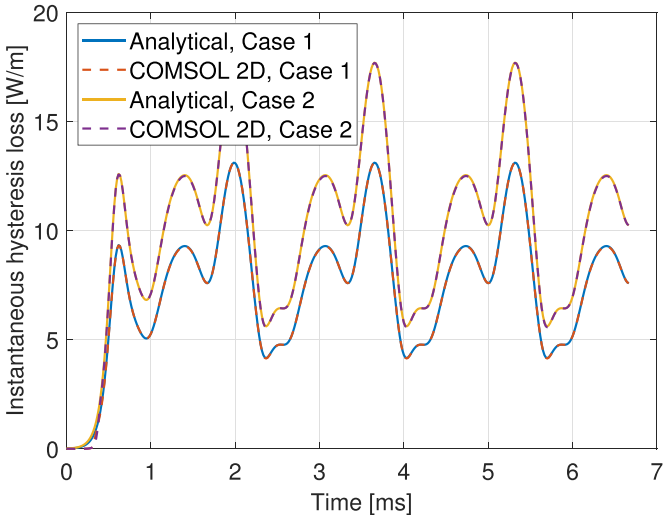

Figure C2. Instantaneous hysteresis loss of a hollow filament (Case 1) and a composite filament (Case 2) in isolation in air due to an external magnetic field, calculated by analytical means and 2D COMSOL simulations.

The electric field in the composite filament is still given by (32).

The instantaneous power loss per unit volume (in $\mathrm{W\,m^{-3}}$) of the composite filament is

$$\begin{aligned}\frac{P_c}{V} &= \frac{1}{\pi R_{\mathrm{fil}}^2}\left(\int_0^{2\pi}\int_0^{R_i}\mathbf{E}\cdot\mathbf{J}\,r\,\mathrm{d}r\,\mathrm{d}\theta+\int_0^{2\pi}\int_{R_i}^{R_{\mathrm{fil}}}\mathbf{E}\cdot\mathbf{J}\,r\,\mathrm{d}r\,\mathrm{d}\theta\right)\\ &= \frac{1}{\pi R_{\mathrm{fil}}^2}\left(J_{c2}\mu_0\int_0^{2\pi}\int_0^{R_i}|\dot{H}_{a,y}\cos\theta-\dot{H}_{a,x}\sin\theta|r^2\,\mathrm{d}r\,\mathrm{d}\theta\right.\\ &\quad\left.+J_{c1}\mu_0\int_0^{2\pi}\int_{R_i}^{R_{\mathrm{fil}}}|\dot{H}_{a,y}\cos\theta-\dot{H}_{a,x}\sin\theta|r^2\,\mathrm{d}r\,\mathrm{d}\theta\right)\\ &= \frac{1}{\pi R_{\mathrm{fil}}^2}\left(J_{c2}K\int_0^{R_i}r^2\,\mathrm{d}r+J_{c1}K\int_{R_i}^{R_{\mathrm{fil}}}r^2\,\mathrm{d}r\right)\\ &= \frac{R_{\mathrm{fil}}}{3\pi}K\left(J_{c1}\left(1-\left(\frac{R_i}{R_{\mathrm{fil}}}\right)^3\right)+J_{c2}\left(\frac{R_i}{R_{\mathrm{fil}}}\right)^3\right),\end{aligned}\tag{C2}$$

where K is the same as defined in (36).

If the inner cylinder is instead an empty space, for example, the hollow space left behind in IMD, J_{c2} can be set as 0 [8].

To verify the above analytical method, we compare the results with 2D COMSOL simulations as we calculate the instantaneous hysteresis loss of the two composite wires, labelled 'Case 1' and 'Case 2', respectively, and described in table C1. These wires are subject to the external magnetic field B_x and B_y given in (72) and (73), respectively, with the amplitude factor $k=5$. We choose $k=5$ to ensure full penetration of the external field. The geometry of the wires is shown in figure C1. The instantaneous hysteresis losses are shown in figure C2, exhibiting very good agreement between the analytical and numerical methods.

Appendix D. Results with $E_0 = 10^{-4}$ V m^{-1}

The critical electric field used in COMSOL simulations for hysteresis loss in the main text is $E_0 = 10^{-5}\ \mathrm{V\,m^{-1}}$, as stated in table 2. If $E_0 = 10^{-4}\ \mathrm{V\,m^{-1}}$ is used instead, the hysteresis loss as the amplitude and frequency of the external magnetic field vary are given in figures D1(a) and (b), respectively.

From figure D1(a), the numerical results for hysteresis loss move slightly closer to the analytical ones at low amplitudes when $E_0 = 10^{-4}\ \mathrm{V\,m^{-1}}$, but are still very far from the analytical results.

From figure D1(b), the numerical results for hysteresis loss at low frequencies are lower and further away from the analytical results for the case $E_0 = 10^{-4}\ \mathrm{V\,m^{-1}}$ compared to $E_0 = 10^{-5}\ \mathrm{V\,m^{-1}}$. This is because, although the electric field strength E_z in the filament induced by a given external magnetic field is the same for the two E_0, the magnitude of the current density is larger for the case when $E_0 = 10^{-5}\ \mathrm{V\,m^{-1}}$. This is because with the J–E relationship in (66) in the QCSM model, a smaller E_0 leads to a larger $|J_z|$ for a given E_z. Since power dissipation is proportional to J_zE_z, larger J_z with the same E_z leads to a larger loss.

It is only at low frequency of the external magnetic field that the numerically simulated hysteresis losses are below the analytical results. This is because when the frequency is low, E_z induced is low, and $|J_z|$ may not reach J_c according to (66), especially for a larger E_0; but at high frequency, E_z induced is higher, and $|J_z|$ would reach J_c in the QCSM in the numerical models. In the critical state model, $|J_z| = J_c$ whenever there is nonzero E_z.

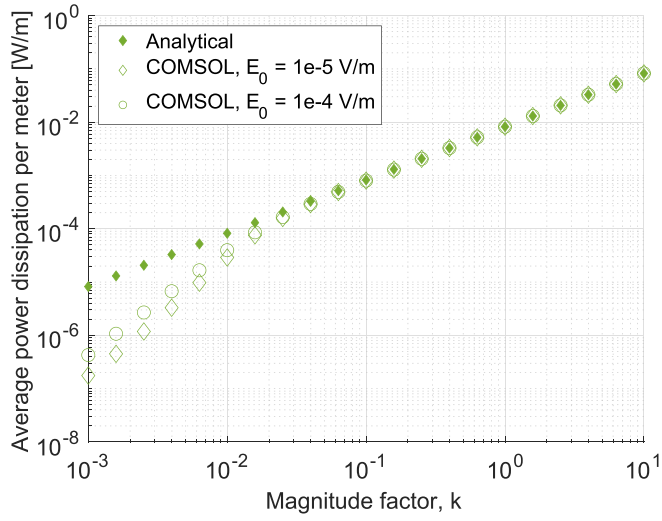

(a)

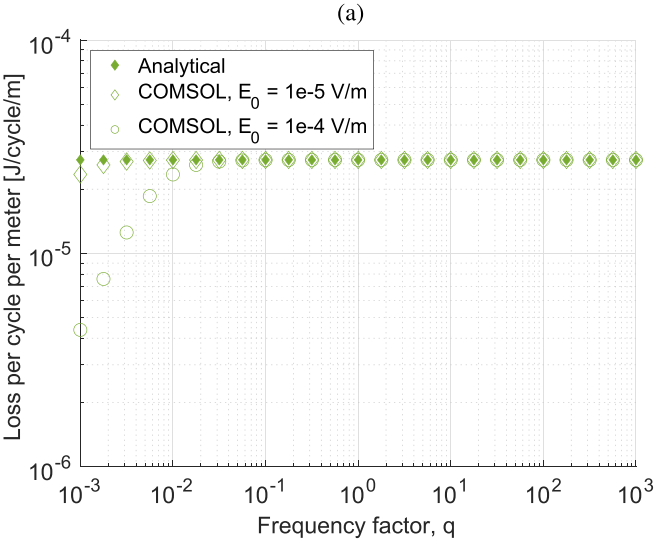

(b)

Figure D1. Average power dissipation per meter of an MgB_2 filament due to hysteresis loss as the (a) amplitude and (b) frequency of the external magnetic field are varied, according to the analytical calculation and COMSOL simulations with different E_0.

ORCID iDs

Calvin C T Chow https://orcid.org/0000-0002-8703-5104
Mark D Ainslie https://orcid.org/0000-0003-0466-3680
K T Chau https://orcid.org/0000-0003-1620-9688

References

[1] Kalsi S S, Badcock R, Storey J, Hamilton K A and Jiang Z 2021 Motors employing REBCO CORC and MgB_2 superconductors for ac stator windings *IEEE Trans. Appl. Supercond.* **31** 5206807
[2] Corduan M, Boll M, Bause R, Oomen M P, Filipenko M and Noe M 2020 Topology comparison of superconducting ac machines for hybrid electric aircraft *IEEE Trans. Appl. Supercond.* **30** 5200810
[3] Chow C C T, Ainslie M D and Chau K T 2023 High temperature superconducting rotating electrical machines: an overview *Energy Rep.* **9** 1124–56
[4] Santos B M O, Dias F J M, Trillaud F, Sotelo G G and de Andrade R 2023 A review of technology readiness levels for superconducting electric machinery *Energies* **16** 5955
[5] Qiao Y, Ainslie M D, Sun Y, Badcock R A, Strickland N M and Jiang Z 2025 3D numerical simulation of magnetization loss in multifilamentary MgB_2 wires at 20 K *Supercond. Sci. Technol.* **38** 015024
[6] Sumption M D 2019 AC loss of superconducting materials-refined loss estimates of MgB_2 wires for superconducting motors and generators *Proc. AIAA Propulsion Energy 2019 Forum* (*Indianapolis, IN, USA, 19–22 August 2019*) (https://doi.org/10.2514/6.2019-4495)
[7] Zhou C, Miyoshi Y, van Lanen E P A, Dhallé M and Nijhuis A 2012 Inter-filament resistance, effective transverse resistivity and coupling loss in superconducting multi-filamentary NbTi and Nb_3Sn strands *Supercond. Sci. Technol.* **25** 015013
[8] Carr W J 2001 *AC Loss and Macroscopic Theory of Superconductors* 2nd edn (Taylor & Francis Inc.)
[9] Turck B 1979 Coupling losses in various outer normal layers surrounding the filament bundle of a superconducting composite *J. Appl. Phys.* **50** 5397–401
[10] Zhao J, Li Y and Gao Y 2017 3D simulation of ac loss in a twisted multi-filamentary superconducting wire *Cryogenics* **84** 60–68
[11] Klimenko E Y, Chechetkin V R, Khayrutdinov R R and Solodovnikov S G 2010 Electrodynamics of multifilament superconductors *Cryogenics* **50** 359–65
[12] Escamez G, Sirois F, Lahtinen V, Stenvall A, Badel A, Tixador P, Ramdane B, Meunier G, Perrin-Bit R and Bruzek C-E 2016 3-D numerical modeling of AC losses in multifilamentary MgB_2 wires *IEEE Trans. Appl. Supercond.* **26** 4701907
[13] Arsenault A, de Sousa Alves B and Sirois F 2021 COMSOL implementation of the H-ϕ-formulation with thin cuts for modeling superconductors with transport currents *IEEE Trans. Appl. Supercond.* **31** 6900109
[14] Kameni A, Makong L, Bouillault F and Masson P J 2019 Reduced model to compute ac losses of twisted multifilamentary superconductors *IEEE Trans. Appl. Supercond.* **29** 5901306
[15] Lyly M, Stenvall A and Mikkonen R 2012 Validation of homogenized filament bundle model in ac loss computations *IEEE Trans. Appl. Supercond.* **22** 4705505
[16] Dular J, Henrotte F, Nicolet A, Wozniak M, Vanderheyden B and Geuzaine C 2024 Helicoidal transformation method for finite element models of twisted superconductors *IEEE Trans. Appl. Supercond.* **34** 8200615
[17] Balachandran T, Salk N J, Lee D, Sumption M D and Haran K S 2022 Methods of estimating ac losses in superconducting MgB_2 armature windings with spatial and time harmonics *IEEE Trans. Appl. Supercond.* **32** 4702407
[18] Balachandran T and Haran K S 2023 Instantaneous loss integration method to estimate ac losses in superconductors with spatial and time harmonics *IEEE Trans. Appl. Supercond.* **33** 5900907
[19] Ries G 1977 AC-losses in multifilamentary superconductors at technical frequencies *IEEE Trans. Magn.* **13** 524–6
[20] Farlow S J 1993 *Partial Differential Equations for Scientists and Engineers* (Dover Publications)
[21] Zermeno V M R, Grilli F and Sirois F 2013 A full 3D time-dependent electromagnetic model for Roebel cables *Supercond. Sci. Technol.* **26** 052001
[22] Grilli F, Pardo E, Morandi A, Gomory F, Solovyov M, Zermeno V M R, Brambilla R, Benkel T and Riva N 2021 Electromagnetic modeling of superconductors with commercial software: possibilities with two vector potential-based formulations *IEEE Trans. Appl. Supercond.* **31** 5900109
[23] Weisstein E W Erf. MathWorld–A Wolfram web resource (available at: https://mathworld.wolfram.com/Erf.html) (Accessed 267 October 2021)
[24] Felder J L, Brown G V, Kim H D and Chu J 2011 Turboelectric distributed propulsion in a hybrid wing body aircraft *Presented at the 20th Int. Soc. Airbreathing Engines (ISABE 2011) (Gothenburg, Sweden, 12–16 October 2011)* (available at: https://ntrs.nasa.gov/citations/20120000856)
[25] Lubin T 2020 Analytical modeling and design of HTS machines (available at: https://hal.science/hal-03015447/)
[26] Corduan M 2020 Design of superconducting AC machines for hybrid-electric aircraft *PhD Dissertation* Dept. Elect. Eng. Inf. Technol., Karlsruhe Inst. Technol Karlsruhe, Germany (https://doi.org/10.5445/IR/1000129218)
[27] Qiao Y, Rindfleisch M, Tomsic M, Sumption M D, Amemiya N, Badcock R A, Strickland N M and Jiang Z 2023 I_c measurement of twisted multifilamentary MgB_2 wires with non-magnetic sheath over a wide range of temperatures and fields *Superconductivity* **8** 100072
[28] Sumption M D 2018 AC loss of superconducting materials in motors and generators for very high density motors and generators for hybrid-electric aircraft *Proc. 2018 AIAA/IEEE Electric Aircraft Technol. Symp.* (*Cincinnati, OH, USA, 9–11 July 2018*) (https://doi.org/10.2514/6.2018-5001)
[29] Balachandran T, Lee D, Salk N and Haran K S 2020 A fully superconducting air-core machine for aircraft propulsion *IOP Conf. Ser.: Mater. Sci. Eng.* **756** 012030
[30] Terao Y, Kong W, Ohsaki H, Oyori H and Morioka N 2018 Electromagnetic design of superconducting synchronous motors for electric aircraft propulsion *IEEE Trans. Appl. Supercond.* **28** 5208005
[31] Terao Y, Nakamura H, Okumura S, Fuchino S and Ohsaki H 2023 AC loss of MgB_2 superconducting coils with alternating transport current in rotating magnetic field *IEEE Trans. Appl. Supercond.* **33** 3600305
[32] Manolopoulos C 2019 Superconducting machines for aerospace electric propulsion systems *PhD Thesis* Dept. Elect. Electron. Eng Univ. Manchester (available at: https://uom-qa.qa.elsevierpure.com/ws/portalfiles/portal/353790332/FULL_TEXT.PDF)
[33] Ye S and Kumakura H 2016 The development of MgB_2 superconducting wires fabricated with an internal Mg diffusion (IMD) process *Supercond. Sci. Technol.* **29** 113004

[34] Uchiyama D, Mizuno K, Akao T, Maeda M, Kawakami T, Kobayashi H, Kubota Y and Yasohama K 2007 Fibrous structure and critical current density of MgB_2 superconducting wire *Cryogenics* **47** 282–6
[35] Susner M A, Daniels T W, Sumption M D, Rindfleisch M A, Thong C J and Collings E W 2012 Drawing induced texture and the evolution of superconductive properties with heat treatment time in powder-in-tubein situprocessed MgB_2 strands *Supercond. Sci. Technol.* **25** 065002
[36] Gajda D *et al* 2024 The influence of Sm_2O_3 dopant on structure, morphology and transport critical current density of MgB_2 wires investigated by using the transmission electron microscope *J. Magnesium Alloys* **12** 5061–78
[37] Gajda D, Babij M, Zaleski A, Avci D, Karaboga F, Yetis H, Belenli I and Czujko T 2024 Investigation of layered structure formation in MgB_2 wires produced by the internal Mg coating process under low and high isostatic pressures *Materials* **17** 1362
[38] Gajda D, Zaleski A J, Morawski A J, Babij M, Szymański D, Gajda G, Rindfleisch M A, Shahbazi M and Hossain M S A 2021 Superior engineering critical current density obtained via hot isostatic pressing of MgB_2 wires manufactured using nano-amorphous isotopic boron *J. Alloys Compounds* **871** 159579
[39] Li G Z, Sumption M D, Susner M A, Yang Y, Reddy K M, Rindfleisch M A, Tomsic M J, Thong C J and Collings E W 2012 The critical current density of advanced internal-Mg-diffusion-processed MgB_2 wires *Supercond. Sci. Technol.* **25** 115023
[40] Brunner B 2016 MgB_2 wires made by diffusion method and their properties: Summary of doctoral dissertation *PhD Dissertation* (available at: www.fei.stuba.sk/buxus/docs/2016/autoreferaty/Autoref_Brunner.pdf)
[41] Hur J M, Togano K, Matsumoto A, Kumakura H, Wada H and Kimura K 2008 Fabrication of high-performance MgB_2 wires by an internal Mg diffusion process *Supercond. Sci. Technol.* **21** 032001
[42] Yetiş H *et al* 2022 Transport and structural properties of MgB_2/Fe wires produced by redesigning internal Mg diffusion process *Supercond. Sci. Technol.* **35** 045012
[43] Li G Z, Sumption M D, Zwayer J B, Susner M A, Rindfleisch M A, Thong C J, Tomsic M J and Collings E W 2013 Effects of carbon concentration and filament number on advanced internal Mg infiltration-processed MgB_2 strands *Supercond. Sci. Technol.* **26** 095007
[44] Chow C C T, Zhang M and Chau K T 2025 Analytical AC loss comparison between REBCO, MgB_2, Copper, and aluminum litz wires for cryogenic electrical machines *IEEE Trans. Appl. Supercond.* **35** 5201416
[45] Qiao Y, Ainslie M, Sun Y, Rindfleisch M, Badcock R A, Strickland N M and Jiang Z 2025 3D simulations of total AC loss in a twisted multifilamentary MgB_2 wire carrying AC currents under AC magnetic fields at 20 K *Supercond. Sci. Technol.* **38** 055027